Scalable AIE Emitters for Luminescent Solar Concentrators: the Role of Fluorination

Andrea Nitti,[a,†] Elisavet Tatsi,[b,†] Enrico Magnani,[a] Giuseppe Mattioli,[c] Francesco Porcelli,[c] Chiara Botta,[d] Gianmarco Griffini,*[,b] and Dario Pasini,*[,a]

Table of Contents

1. Synthesis and characterization

All commercially available reagents and solvents were purchased from Sigma-Aldrich, Fluorochem and Alfa Aesar. They were all used as received. Naphthothiophene compounds were synthesized according to literature.[S1] Flash chromatography was carried out using Merck silica gel 60 (pore size 60 Å, 270-400 Mesh). ^{1}H and ^{13}C NMR spectra were recorded from solutions in deuterated solvents on 400 Bruker spectrometers with the residual solvent as the internal standard. Mass spectra of pure compounds were recorded using a Bruker Autoflex MALDI-TOF in positive reflectron mode with or without trans-2-(3-(4-tert-Butylphenyl)-2-methyl-2-propenylidene)malononitrile (DCTB) as the matrix. The spectra were recorded also without the matrix, giving in most cases equivalent results due to the direct formation of the radical cation of the relevant species.[S2] Differential scanning calorimetry (DSC) analyses were performed with a DSC 823e Mettler–Toledo instrument. The samples of 8 mg were subjected to a thermal cycle from 30 °C to 200 °C with heating rate of 10 °C min^{-1}.

Synthesis of New Compounds

Compound 1.

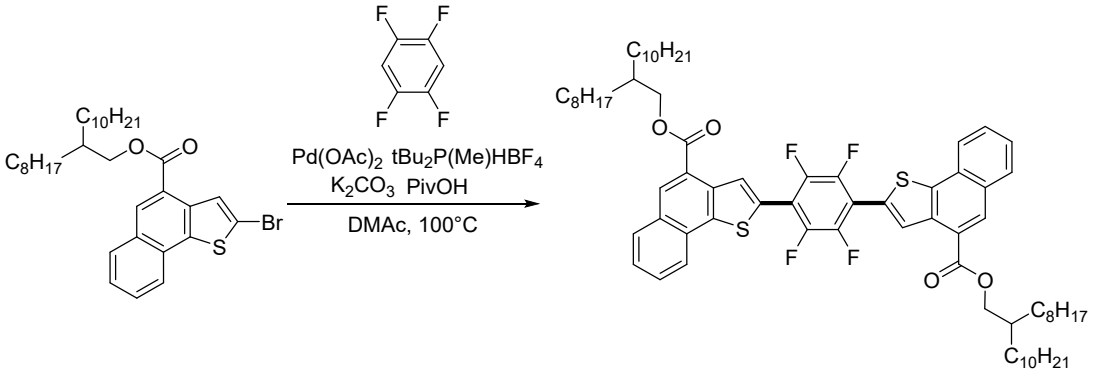

In a Schlenk tube dried under argon atmosphere were added in sequence 1,2,4,5-tetrafluorobenzene (55.9 µL, 0.5 mmol, 1 eq), 2-octyldodecyl 2-bromonaphtho[1,2-*b*]thiophene-4-carboxylate (588 mg,

1 mmol, 2 eq), pivalic acid (25 μL, 2.5 mmol, 5 eq) and DMAc (2.5 mL, 0.2 M). Reaction mixture was degassed for 10 min, then $Pd(OAc)_2$ (11 mg, 0.05 mmol, 0.1 eq), $^tBu_2P(Me)\cdot HBF_4$ (25 mg, 0.1 mmol, 0.2 eq) and K_2CO_3 (207 mg, 1.5 mmol, 3 eq) were added in one portion. Reaction mixture was degassed for another 5 min, warmed to 100°C and kept at the same temperature for 48 h. After TLC monitoring, reaction solvent was removed under reduced pressure and the crude purified by flash chromatography (SiO_2; petroleum ether:DCM 8:2) as eluent. Compound **1** was obtained as brilliant yellow powder (396 mg, 68%). ^{1}H NMR (400 MHz, $CDCl_3$) δ: 8.92 (s, 2H), 8.56 (s, 2H), 8.18 (d, J = 7.9 Hz, 2H), 8.01 (d, J = 8.1 Hz, 2H), 7.69 (t, J = 7.5 Hz, 2H), 7.59 (t, J = 7.5 Hz, 2H), 4.41 (d, J = 5.7 Hz, 4H), 1.97 – 1.88 (m, 2H), 1.61 – 1.16 (m, 64H), 0.84 (t, J = 7.0, 12H). ^{19}F NMR (376 MHz, $CDCl_3$) δ: -139.3. ^{13}C NMR (101 MHz, $CDCl_3$) δ: 166.4, 145.6, 143.0, 140.1, 134.4, 130.9, 130.2, 130.0, 129. 8, 129.3, 129.1, 127.4, 126. 8, 123.6, 123.5, 113.1, 68.2, 37.4, 31.7, 31.4, 30.7, 29.8, 29.5, 29.2, 26.7, 22.5, 13.9. The data are consistent with those already reported in ref. [S3] HRMS $[M+Na]^+$ calcd. for $C_{72}H_{94}F_4O_4S_2$: 1185.6422; found: 1185.6458.

Compound 2.

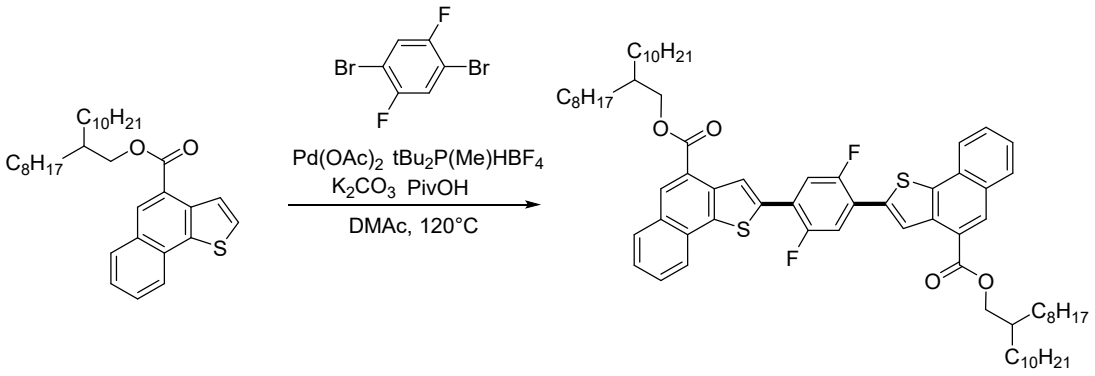

In a Schlenk tube, dried under argon atmosphere, 1,4-dibromo-2,5-difluorobenzene (136 mg, 0.5 mmol, 1 eq), 2-octyldodecyl naphtho[1,2-*b*]thiophene-4-carboxylate (508 mg, 1 mmol, 2 eq), pivalic acid (25 μL, 2.5 mmol, 5 eq) and DMAc (2.5 mL, 0.2 M) were added in sequence. The reaction mixture was degassed for 10 min, then $Pd(OAc)_2$ (11 mg, 0.05 mmol, 0.1 eq), $^tBu_2P(Me)\cdot HBF_4$ (25

mg, 0.1 mmol, 0.2 eq) and K_2CO_3 (138 mg, 1 mmol, 2 eq) were added in one portion. The reaction mixture was degassed for another 5 min, warmed to 120 °C and kept at the same temperature for 24 h. After TLC monitoring, the reaction solvent was removed under reduced pressure and the crude was purified by flash chromatography (SiO_2; petroleum ether:DCM 8:2). Compound **2** was obtained as a brilliant yellow powder in (332 mg, 51%). ^{1}H NMR (400 MHz, $CDCl_3$) δ 8.79 (s, 2H), 8.53 (s, 2H), 8.15 (d, J = 8.2 Hz, 2H), 7.99 (d, J = 8.2 Hz, 2H), 7.72 – 7.62 (m, 4H), 7.57 (t, J = 7.5 Hz, 2H), 4.40 (d, J = 5.7 Hz, 4H), 1.91 (d, J = 6.2 Hz, 2H), 1.52 – 1.10 (m, 84H), 0.85 (s, 6H). ^{13}C NMR (101 MHz, $CDCl_3$) δ 166.4, 145.6, 143.0, 140.1, 134.4, 130.9, 130.2, 130.0, 129. 8, 129.3, 129.1, 127.4, 126. 8, 123.6, 123.5, 113.1, 68.2, 37.4, 31.7, 31.4, 30.7, 29.8, 29.5, 29.2, 26.7, 22.5, 13.9. HRMS $[M+H]^+$ calcd. for $C_{72}H_{96}F_2O_4S_2$: 1127.6791; found: 1127.6826.

Compound 3.

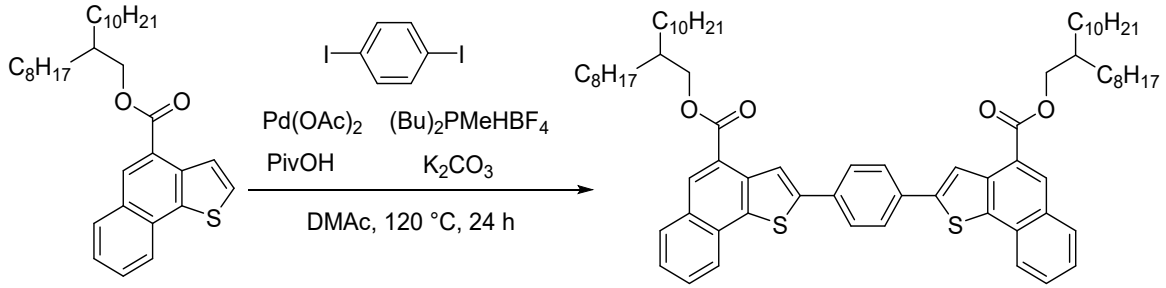

In a Schlenk tube dried under argon atmosphere 1,4-diiodobenzene (165 mg, 0.5 mmol, 1 eq), 2-octyldodecyl naphtho[1,2-*b*]thiophene-4-carboxylate (534 mg, 1.05 mmol, 2.1 eq), K_2CO_3 (207 mg, 1.5 mmol, 3 eq), pivalic acid (282 μL, 2.5 mmol, 5 eq) and DMAc (2.5 mL, 0.2 M) were added in sequence. The reaction mixture was degassed for 10 min, then $Pd(OAc)_2$ (11 mg, 0.05 mmol, 0.1 eq) and $^tBu_2P(Me)\cdot HBF_4$ (25 mg, 0.1 mmol, 0.2 eq) were added in one portion. The reaction mixture was degassed for another 5 min, warmed to 120 °C and kept at the same temperature for 24 h. After TLC monitoring, the reaction solvent was removed under reduced pressure and the crude was purified by flash chromatography (SiO_2; petroleum ether:DCM 8:2). Compound **3** was obtained as a yellow

powder (262 mg, 48%). ^{1}H NMR (400 MHz, $CDCl_3$) δ 8.66 (s, 2H), 8.54 (s, 2H), 8.15 (d, J = 8.2 Hz, 2H), 8.00 (d, J = 8.1 Hz, 2H), 7.89 (s, 4H), 7.68 (d, J = 8.3 Hz, 2H), 7.55 (d, J = 8.2 Hz, 2H), 4.40 (d, J = 5.7 Hz, 4H), 1.96 – 1.87 (m, 2H), 1.60 – 1.13 (m, 64H), 0.90 – 0.76 (m, 6H). ^{13}C NMR (101 MHz, $CDCl_3$) δ 14.2, 22.8, 27.1, 29.5, 29.8, 29.8, 29.9, 30.2, 31.8, 32.1, 37.8, 68.3, 122.1, 123.7, 126.4, 127.1, 129.2, 129.8, 130.5, 130.9, 134.3, 136.5, 138.9, 143.6, 167.0. HRMS $[M+H]^+$ calcd. for $C_{72}H_{98}O_4S_2$: 1091.6979; found: 1091.7009.

Additional Synthetic Experiments

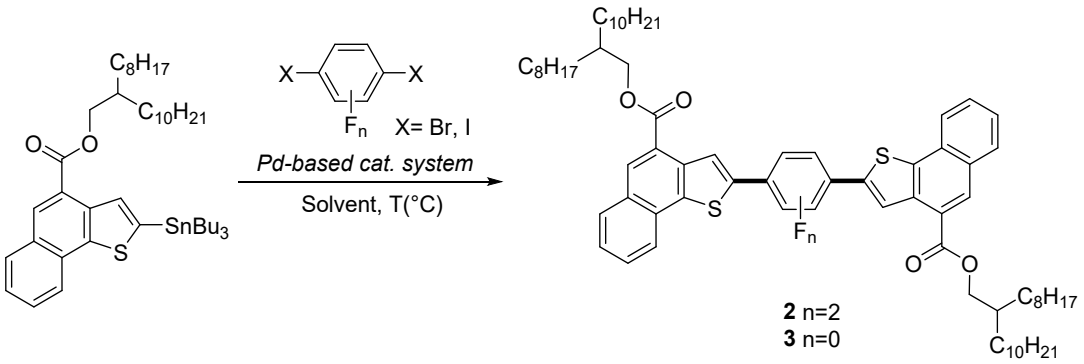

General procedure for Stille coupling. *Example for the synthesis of compound* **3** *(Table S1, entry 3)*. In a Schlenk tube dried under argon atmosphere were added in sequence $PdCl_2(PPh_3)_2$ (10 mg, 0.015 mmol, 5 mol%), 1,4-diiodobenzene (99 mg, 0.3 mmol, 1 eq), 2-octyldodecyl 2-(tributylstannyl)naphtho[1,2-b]thiophene-4-carboxylate (479 mg, 0.6 mmol, 2 eq), and dry Toluene (3 mL, 0.1 M). Reaction mixture was degassed for 20 min, warmed to 110 °C, and kept at the same temperature for 24 h. After TLC monitoring, the reaction solvent was removed under reduced pressure and the crude was purified by flash chromatography with petroleum ether:DCM (8/2) as eluent. Compound **3** was obtained as a yellow powder in 23% yield (75 mg). For compound **2**: Yield 32%.

Table S1. Optimization of experimental conditions for the synthesis of compounds **2** and **3** via DHA protocols.

Compound	Reaction Conditions	Yield (%)
3	$Pd(PPh_3)_4$ 5% mol, Toluene, 110 °C	11
	$Pd(PPh_3)_4$ 5% mol, JohnPhos 10%mol, Toluene, 110 °C	7
	$Pd(OAc)_2$, $(tBu)_2PMe{\cdot}HBF_4$ 20%mol, K_2CO_3, DMF, 100 °C	48
2	$Pd(PPh_3)_4$ 5% mol, Toluene, 110 °C	9
	$Pd(OAc)_2$, $(tBu)_2PMe{\cdot}HBF_4$ 20%mol, K_2CO_3, DMF, 100 °C	51

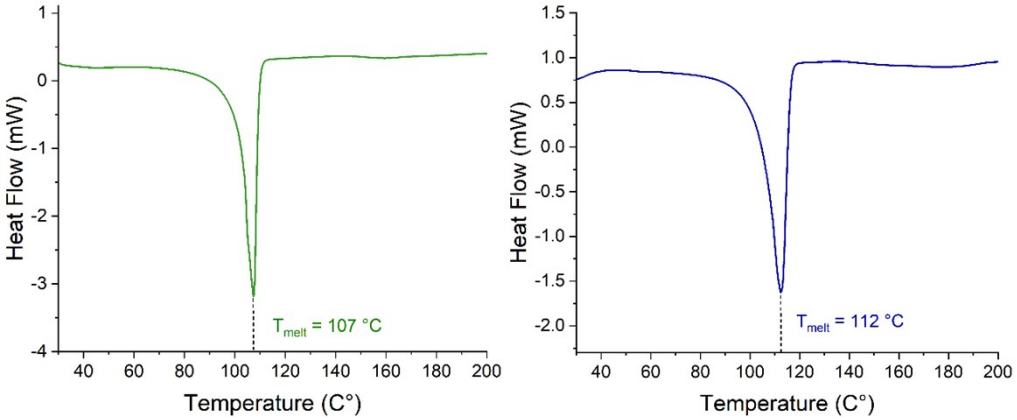

Figure S1. DSC trace of compounds **2** (green) and **3** (blue).

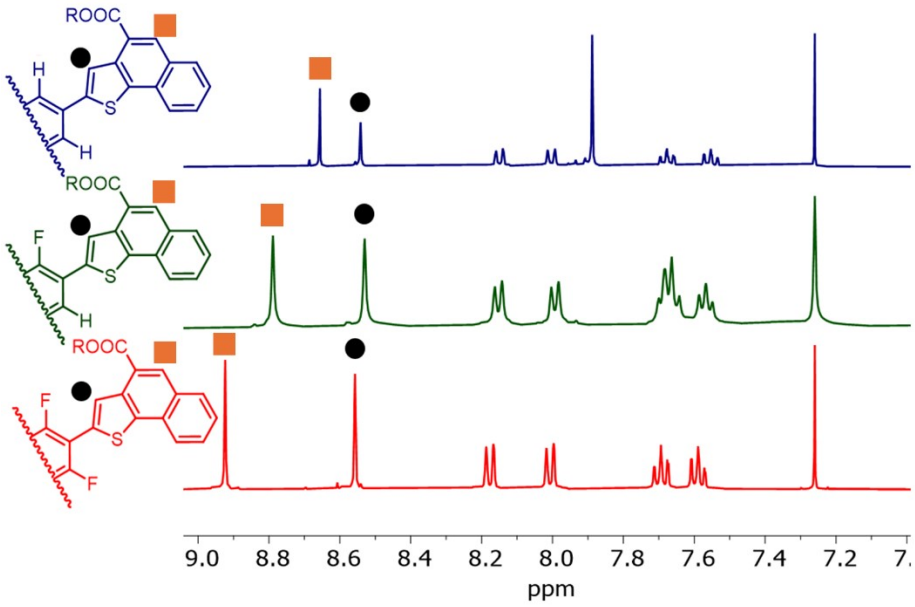

Figure S2. Stacked proton spectra of the aromatic region (in $CDCl_3$) for compounds **1** (red line), **2** (green line) and **3** (blue line).

2. E Factor calculations

Compound 2

compounds	m (g)	waste (g)
1,4-dibromo-2,5-difluorobenzene	0.136	0
2-octyldodecyl naphtho[1,2-*b*]thiophene-4-carboxylate	0.508	0
K_2CO_3	0.138	0.138
pivalic acid	0.250	0.250
$Pd(OAc)_2$	0.011	0.011
$^tBu_2P(Me)\cdot HBF_4$	0.025	0.025
Silica gel	39	39
DMAc	0.250	0
PE	206	0
DCM	103	0
m(g) waste = 39.4 **m(g) of product = 0.332 g** **E-factor= 118**		

Compound 3

compounds	m (g)	waste (g)
1,4-diiodobenzene	0.165	0
2-octyldodecyl naphtho[1,2-*b*]thiophene-4-carboxylate	0.534	0
K_2CO_3	0.207	0.207
pivalic acid	0.250	0.250
$Pd(OAc)_2$	0.011	0.011
$^tBu_2P(Me)\cdot HBF_4$	0.025	0.025
Silica gel	31	31
DMAc	0.250	0
PE	206	0
DCM	103	0
m(g) waste = 31.5 **m(g) of product = 0.262 g** **E-factor= 120**		

3. Absorption and emission spectroscopy

The UV-Vis spectroscopic studies in solutions were recorded using UV-Vis Agilent Cary 60 spectrophotometer. UV–vis absorption spectra of aggregates were recorded on a Thermo Scientific Evolution 600 UV–vis spectrophotometer using wavelength scan with a resolution of 1 nm at a scan speed of 120 nm min^{-1} and a slit width of 2 nm. Steady-state fluorescence spectroscopy of aggregates was performed on a Jasco FP-6600 spectrofluorometer. The photoluminescence experiments and lifetime experiments were recorded using Horiba Fluorolog-3® Model FL3-22iHR. Micrographs of sample nanoaggregates were captured through a Leica DMI3000B fluorescence microscope equipped with a digital camera, by using specific filters based on the excitation and emission wavelengths of the investigated sample. Photoluminescence quantum yield (PLQY) of samples in solid state and **2** or **3**/PMMA coating with optimized concentration (12.5%) were measured with a home-made integrating sphere according to the procedure reported elsewhere.[S3] Time-resolved TCSPC measurements are obtained with PPD-850 single photon detector module and DeltaTime serie DD-300 DeltaDiode and DD-405L DeltaDiode Laser and analysed with the instrument Software DAS6.

Average lifetimes are obtained from multiexponential fits as $\tau_{av} = \sum_i \frac{A_i \tau_i^2}{A_i \tau_i}$

Table S2. Summary table of the photophysical properties of compounds in $CHCl_3$ solutions and as powders

	λ_{abs}(nm)	ε(M^{-1} cm^{-1})	λ_{em}(nm)	τ_{av}(ns)	PLQY(%)	λ_{em}(nm)	τ_{av}(ns)	PLQY(%)
			Solution				*Powder*	
1	298, 360, 382	$4.0 \cdot 10^4$	413, 438, 505	0.564	32	508	3.42	23, 28[a]
2	299, 364, 389	$4.2 \cdot 10^4$	420, 446, 509	0.599	39	503	2.68	25
3	302, 365, 385	$4.2 \cdot 10^4$	420, 446, 516	0.729	35	501	3.11	17

[a] Cast film from both THF and THF/H_2O mixture (f_w=95%), from ref (S3).

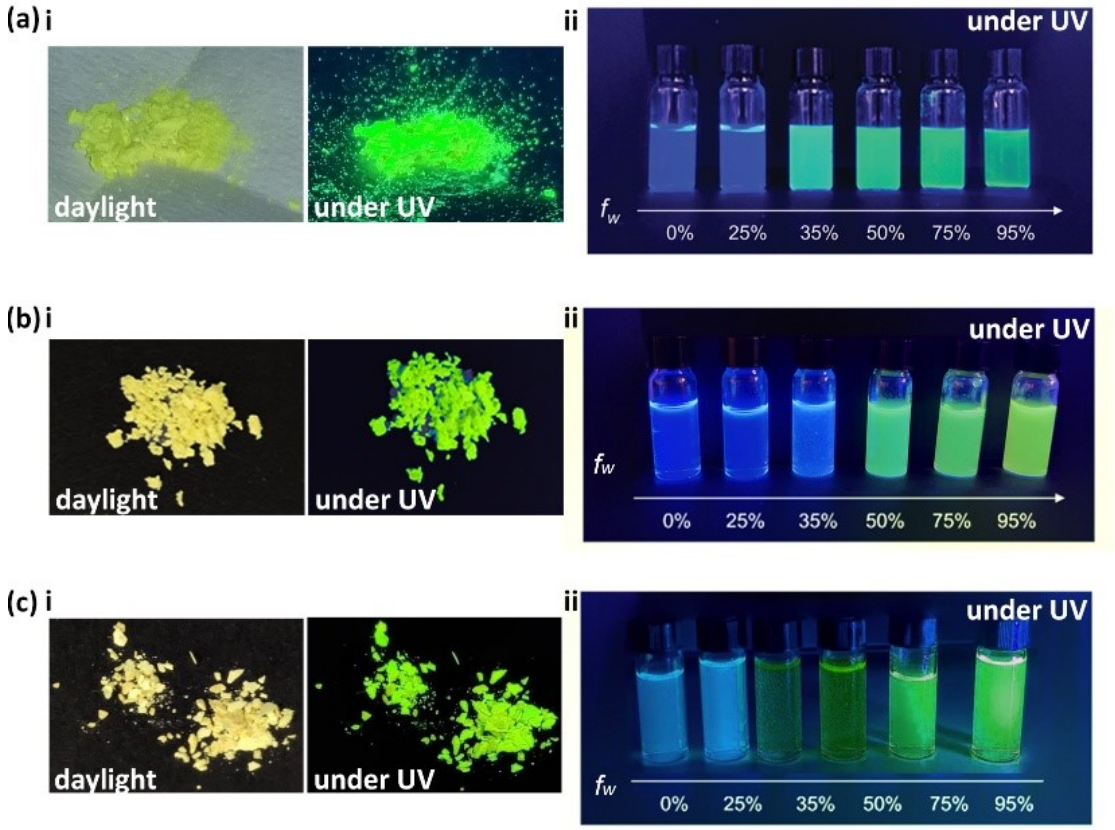

Figure S3. Photographs of compounds **1–3** under different conditions. **(ai–ci)** Images of the powders of compounds **1 (ai)**, **2 (bi)**, and **3 (ci)** under daylight and under UV light (λ_{exc} = 365 nm). **(aii–cii)** Images of the corresponding solutions of compounds **1 (aii)**, **2 (bii)**, and **3 (cii)** under UV light (λ_{exc} = 365 nm) with increasing water content, highlighting the AIE behaviour.

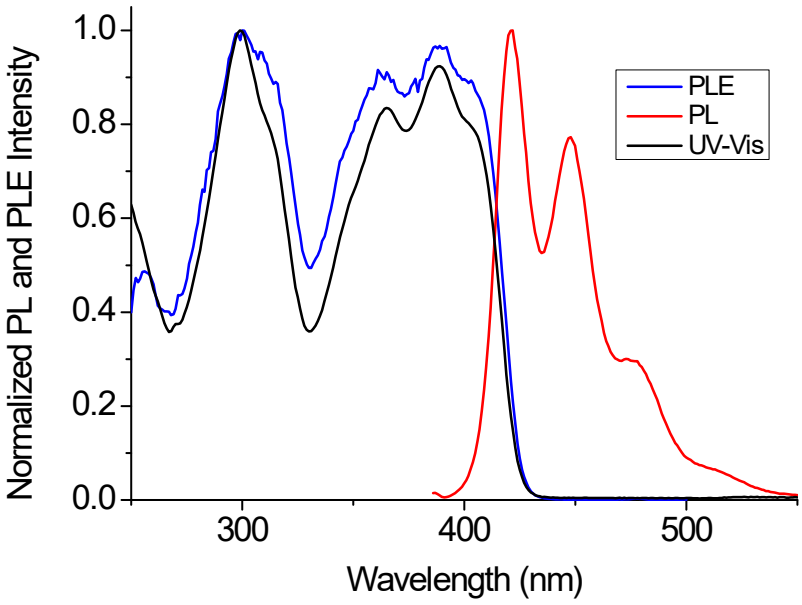

Figure S4. Normalized UV-Vis (black), PLE (blue) and Pl (red) spectra in chloroform (5×10^{-6} M) of compound **1**.

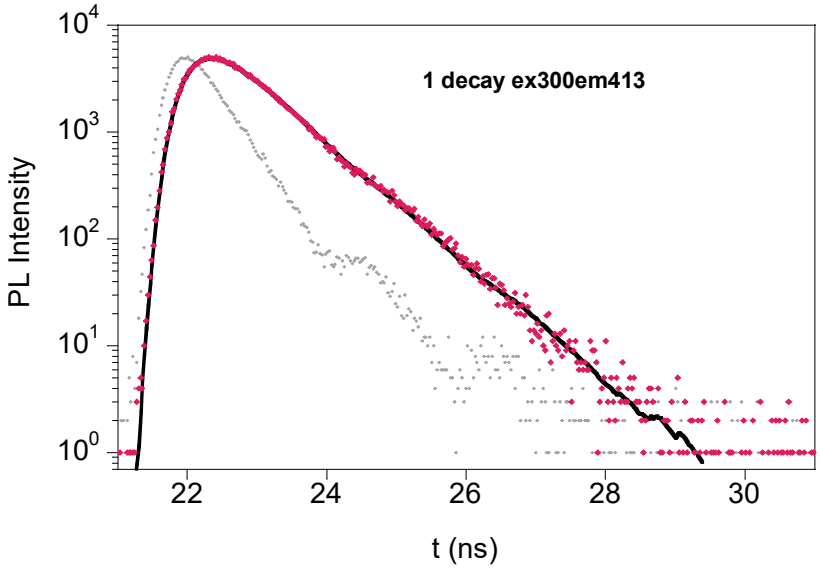

Figure S5. Emission decay at 298 K of compound **1** (red) in Chloroform (5×10^{-6} M) measured at emission wavelength of 413 nm after the pulsed laser excitation at 300 nm (laser prompt in gray). They exhibit biexponential decay ($t_1 = 0.37$ns; $t_2 = 0.71$ns; $B_1 = 0.59$; $B_2 = 0.41$; $\chi^2 = 1.247791$) with an average lifetime of 564 ps.

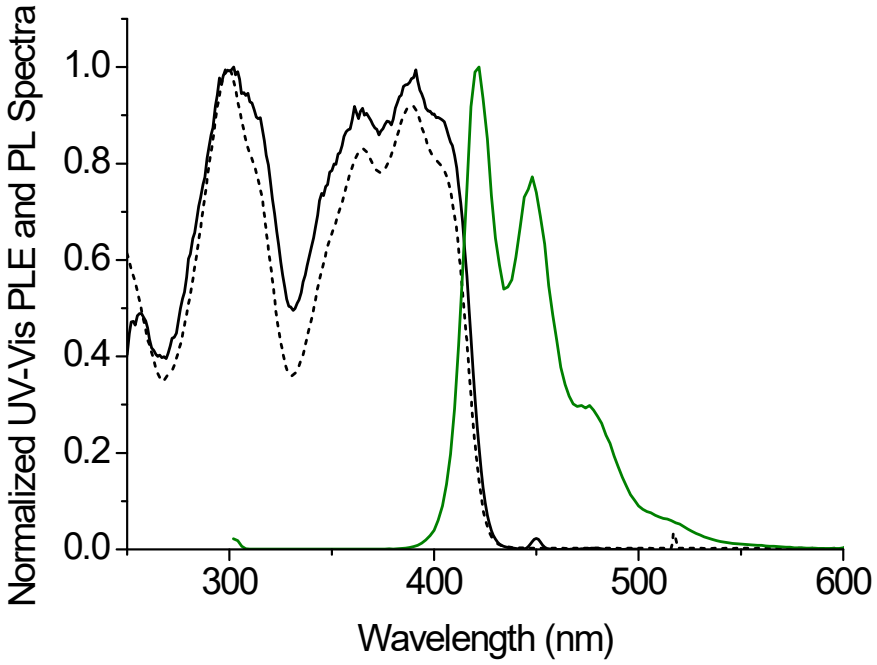

Figure S6. Normalized UV-Vis (black dot line), PLE (black line) and PL (green line) spectra in chloroform (5×10^{-6} M) of compound **2**.

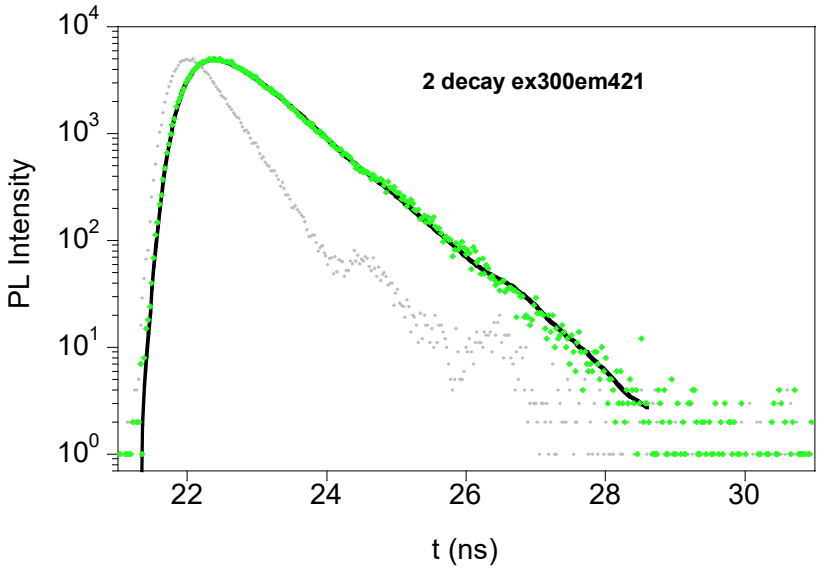

Figure S7. Emission decay at 298 K of compound **2** (green) in Chloroform (5×10^{-6} M) measured at emission wavelength of 421 nm after the pulsed laser excitation at 300 nm (laser prompt in gray). They exhibit biexponential decay ($t_1 = 0.32$ ns; $t_2 = 0.68$ ns; $B_1 = 0.40$; $B_2 = 0.60$; $\chi^2 = 1.489107$) with average lifetime of 599 ps.

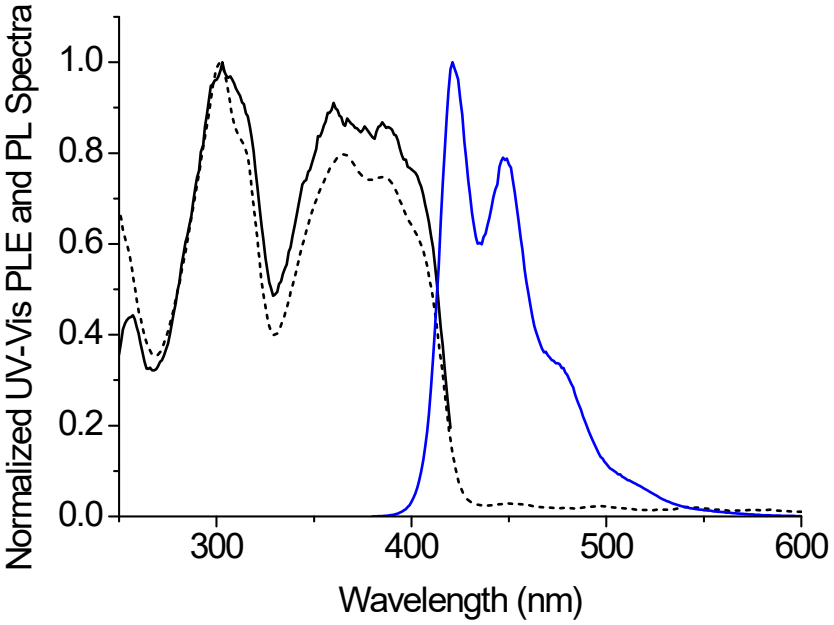

Figure S8. Normalized UV-Vis (black dot line), PLE (black line) and Pl (blue line) spectra in chloroform (5×10^{-6} M) of compound **3**.

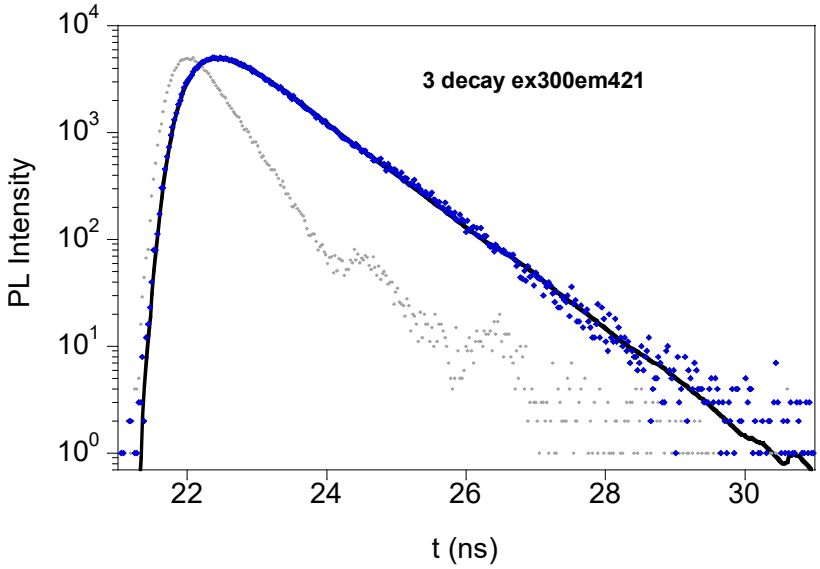

Figure S9. Emission decay at 298 K of compound **3** (blue) in Chloroform (5×10^{-6} M) measured at emission wavelength of 421 nm after the pulsed laser excitation at 300 nm (laser prompt in gray). They exhibit biexponential decay ($t_1 = 0.34$ ns; $t_2 = 0.80$ns; $B_1 = 0.31$; $B_2 = 0.69$; $\chi^2 = 1.289997$) with average lifetime of 729 ps.

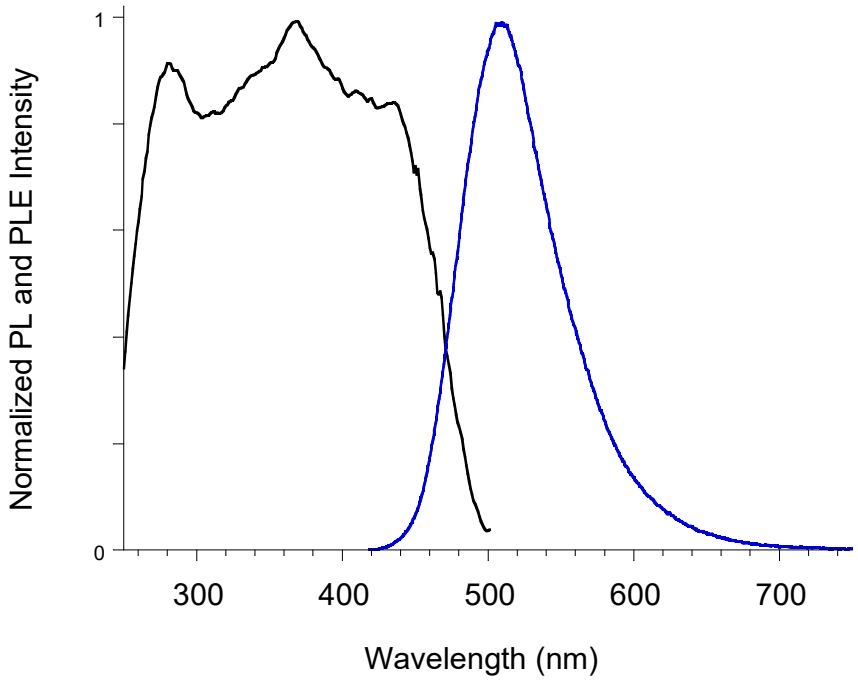

Figure S10. Normalized PLE (black, λ_{em} = 508 nm) and PL (blue, λ_{ex} = 392 nm) spectra for compound **1** in powder.

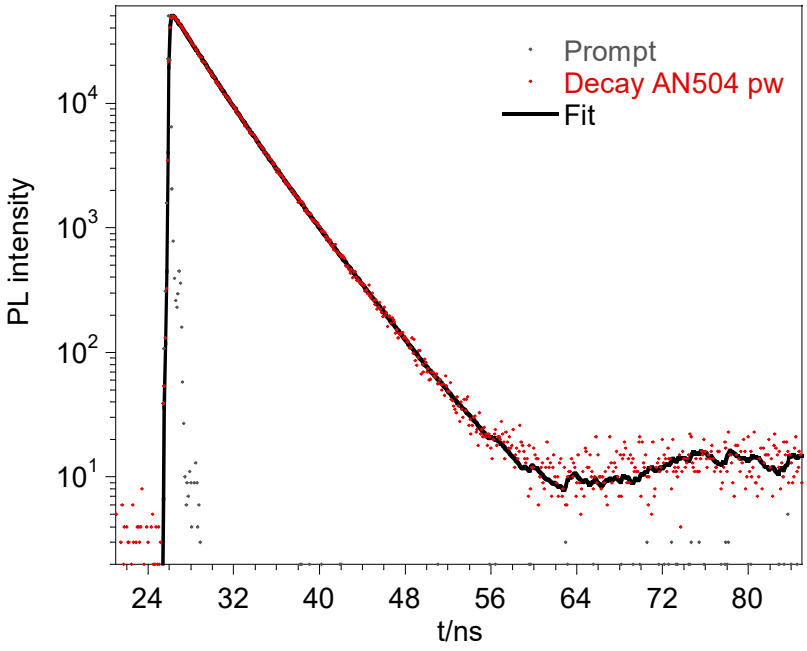

Figure S11. Emission decay at 298 K of compound **1** (red) as a powder measured at emission wavelength of 519 nm after the pulsed laser excitation at 407 nm. Biexponential fit (A_1=0.55, t_1=2.64ns; A_2= 0.45, t_2=4.05ns. χ^2 = 2.445282) with average lifetime of 3.42 ns.

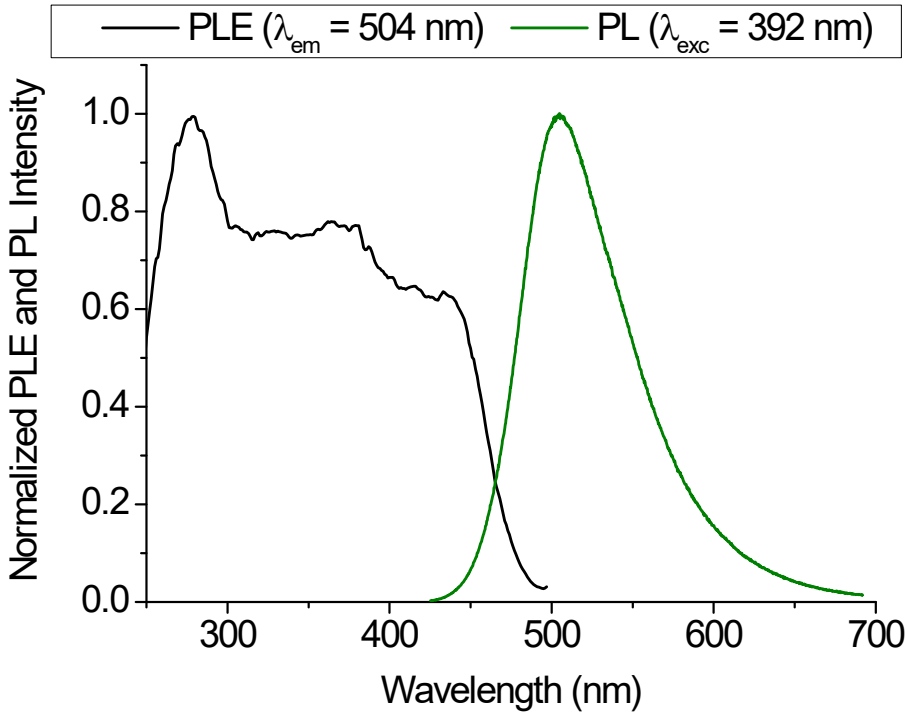

Figure S12. Normalized PLE (black, λ_{em} = 504 nm) and PL (blue, λ_{ex} = 392 nm) spectra for compound **2** in powder.

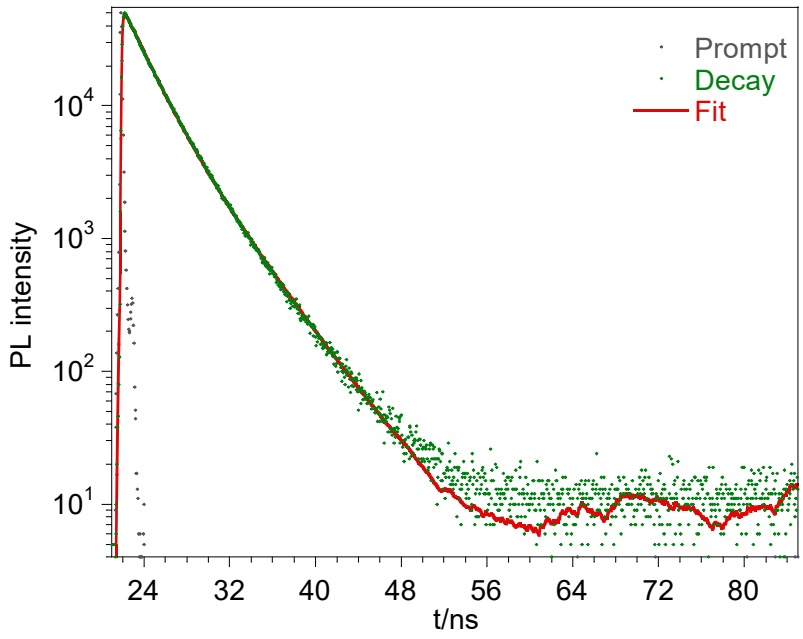

Figure S13. Emission decay at 298 K of compound **2** (green) as a powder measured at emission wavelength of 503 nm after the pulsed laser excitation at 407 nm. Biexponential fit (A_1=0.73, t_1=2.12ns; A_2= 0.27, t_2=4.09ns. χ^2 = 2.021971) with average lifetime of 2.68 ns

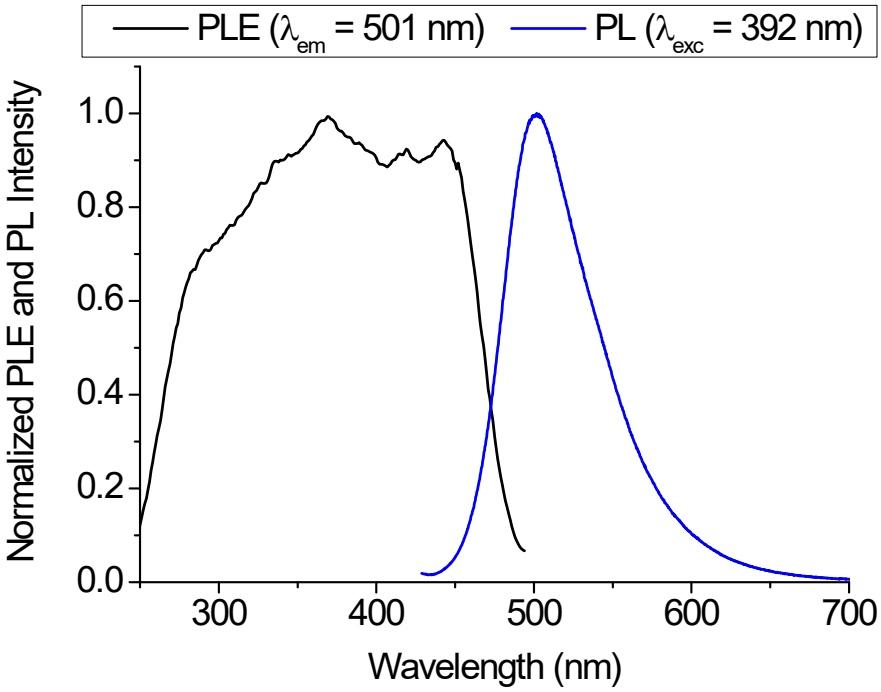

Figure S14. Normalized PLE (black) and PL (green) spectra for compound **3** in powder.

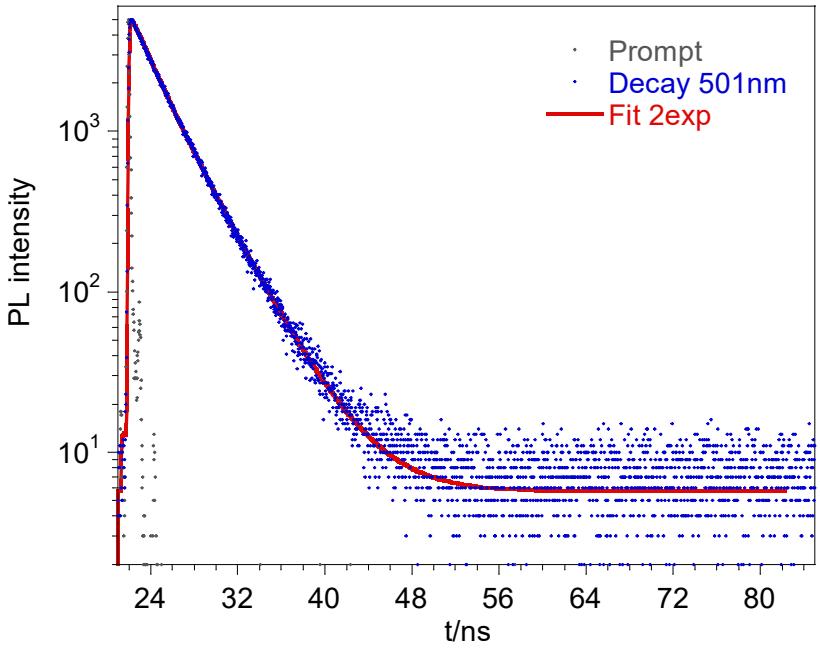

Figure S15. Emission decay at 298 K of compound **3** (blue) as a powder measured at emission wavelength of 501 nm after the pulsed laser excitation at 407 nm. Biexponential fit (A_1=0.41, t_1=1.99ns; A_2= 0.59, t_2=3.55ns. χ^2 = 1.271033) with average lifetime of 3.11 ns

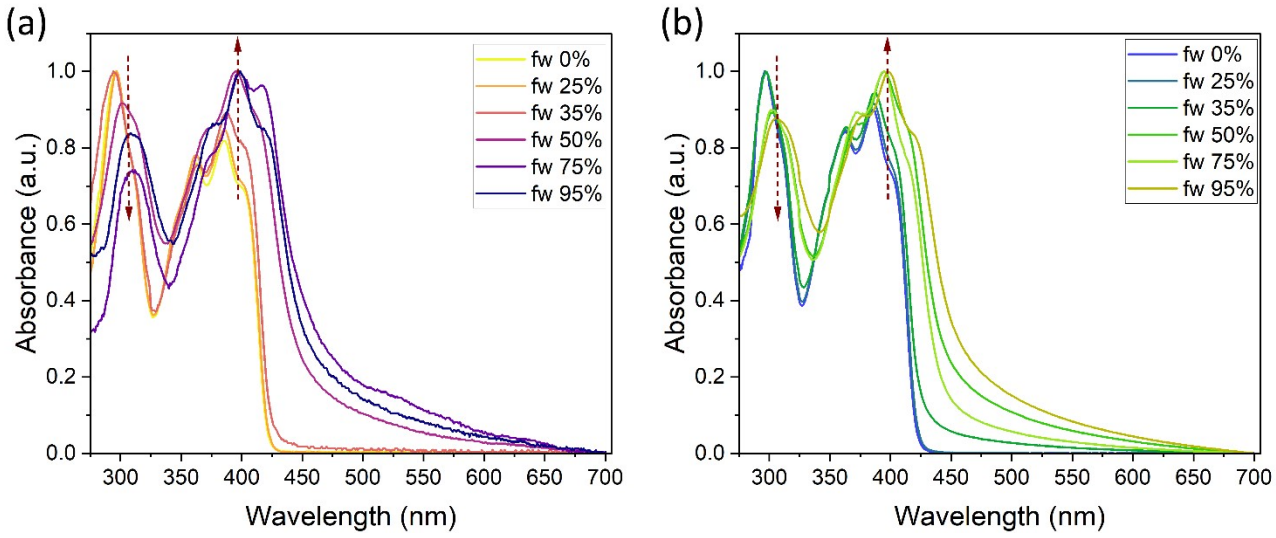

Figure S16. UV-Vis absorption spectra of **(a)** compound **2** and **(b)** compound **3** recorded in THF solutions with increasing water fraction (f_w).

4. Theoretical methods

Atomistic simulations of compounds **1**, **2** and **3** have been performed using a multi-level protocol. The most stable conformers of isolated molecules and molecular dimers have been identified by a conformer-rotamer ensemble sampling tool (CREST) algorithm,[S4] which uses the tight-binding GFN2-xTB Hamiltonian as "engine" for the search of minimum energy configurations.[S5] Electronic and optical properties of the most stable conformers individuated by CREST have been then investigated using (time-dependent) density functional theory simulations, carried out in a Gaussian type orbital (GTO) framework using the ORCA suite of programs.[S6] In detail, Kohn-Sham orbitals have been expanded on the all-electron def2-TZVPP basis set.[S7] The corresponding def2/J basis has been used as an auxiliary basis set for Coulomb fitting in the resolution-of-identity/chain-of-spheres (RIJCOSX) framework for the calculation of Coulomb and exchange integrals implemented in ORCA. In all cases molecules and dimers have been embedded in an implicit THF solvent using a conductor-like polarizable continuum model (CPCM).[S8] Molecular geometries have been fully re-optimized at DFT level using the restricted and regularized hybrid SCAN functional (r^2SCAN0)[S9] as well as the B3LYP functional, to provide better comparison with literaure [B3LYP],[S10] with the addition of the D4 correction for the calculation of dispersion forces.[S11] The absorption vibronic spectra of the investigated molecules have been calculated using time-dependent density functional theory with the r^2SCAN0 functional and the same basis sets, in the framework of the excited state dynamics (ESD) module implemented in ORCA.[S12] Due to the large relaxation of S1 excited states in quinoidal structures, a vertical-gradient approximation cannot be used for the calculation of emission within the ESD framework. Emission spectra have been calculated by applying a Voigt broadening to the pure electronic S1→S0 transitions of fully relaxed S1 states of monomers and dimers, instead. In all cases, a large basis of 600 (1200) vectors connecting occupied and unoccupied eigenstates has been used to build the Davidson expansion space for the calculations of the first 30 electronic transitions of all the molecules (dimers).

Table S3. Frontier orbitals of 1, 2 and 3, calculated using the r^2SCAN0 and B3LYP functionals; Electronic transitions between the ground S0 and first excited S1 electronic states, calculated in the case of monomers (vertical and adiabatic excitations) and dimers (adiabatic excitations); bond lengths and bond orders of C-C bonds connecting benzene and thiophene units of the molecules.

r^2SCAN0 B3LYP	**Frontier orbitals (eV)**		**S0→S1 electronic transitions (nm)**			**Benzene-Thiophene C-C bonds**	
			monomer		***dimer***	Length (Å) S0/S1	Bond order S0/S1
	HOMO	LUMO	vertical	adiabatic	adiabatic		
1 ***(4F)***	-6.26 -5.87	-2.28 -2.32	379	453	542	1.45/1.41	0.92/1.14
2 ***(2F,2H)***	-6.10 -5.69	-2.19 -2.21	387	477	540	1.45/1.40	0.92/1.18
3 ***(4H)***	-5.95 -5.53	-2.13 -2.15	377	478	539	1.45/1.40	0.86/1.16

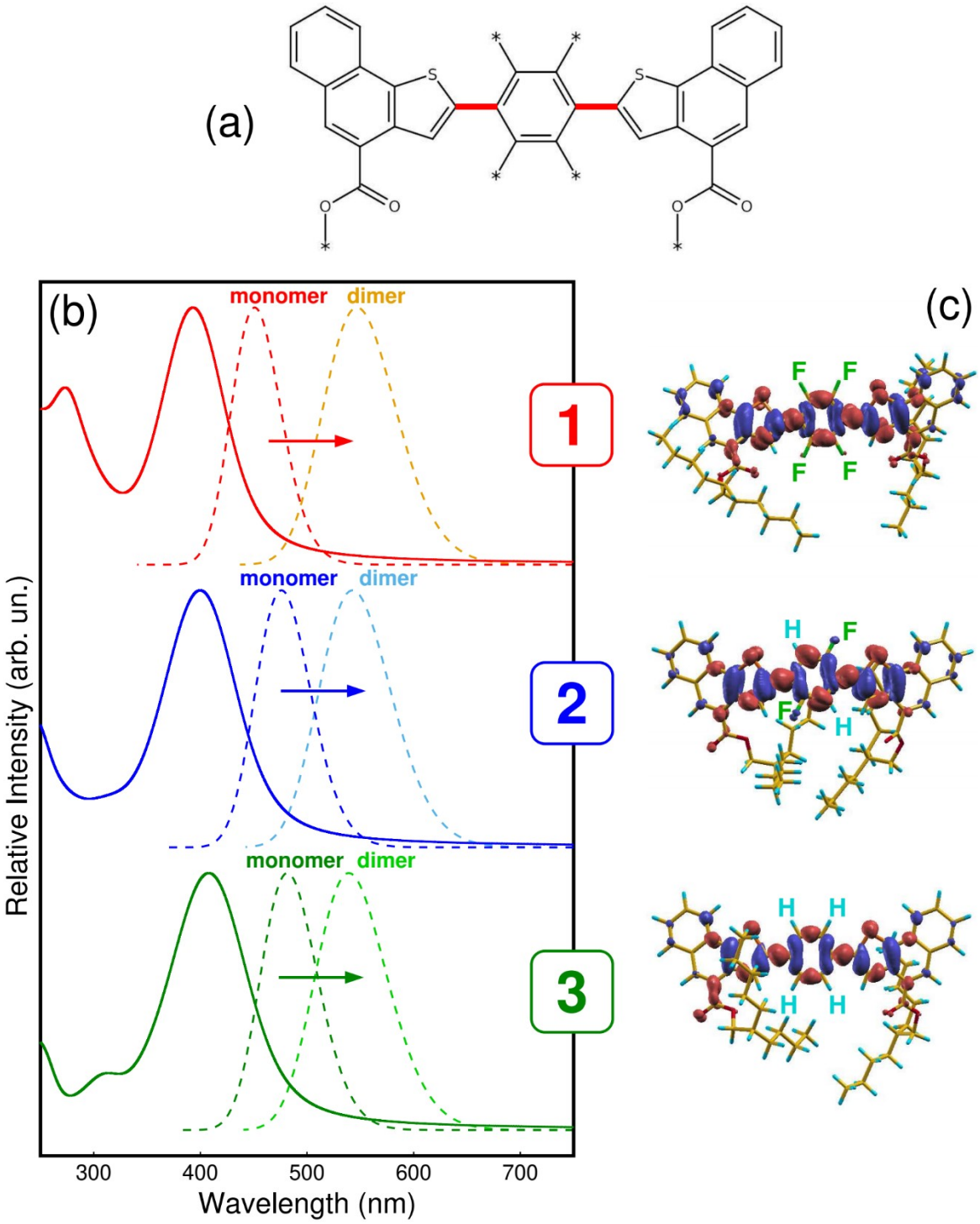

Figure S17. (a) Sketch of the generic structure of compounds **1-3** highlighting C-C bonds connecting benzene and thiophene groups, whose lengths and bond orders are reported in Table S3 and discussed in the main text. (b) TDDFT absorption (full lines) and emission (monomers: dark dashed lines; dimers: pale dashed lines) spectra calculated for compounds **1-3** using the r^{2}SCAN0 functional. (c) Density-difference maps between the S0 ground state and the first S1 excited state of compounds **1-3**. Charge density is displaced from blue regions to red regions upon S0→S1 excitation.

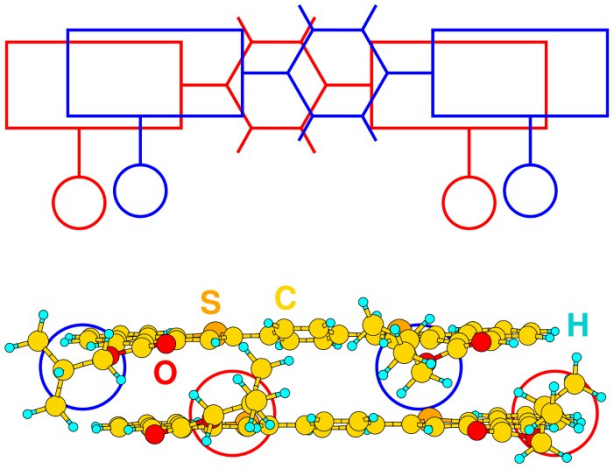

Figure S18. (b) Typical stable structure of molecular dimers. The bulky -COOR tails indicated by red and blue circles prevent a perfect cofacial alignment of the molecules in dimers.

5. LSC devices

Photoluminescence (PL) spectra of LSC matrix samples were recorded in front-face emission configurations and the excitation and emission slits were adjusted so that the maximum emission intensity was within the range of linear response of the detector. Internal and external photon efficiency (η_{int} and η_{ext}, respectively) measurements were performed by illuminating the top face of the LSC using a Abet Technologies Sun 2000 solar simulator with AM1.5G filter (irradiance of 1000 $W \cdot m^{-1}$) and by collecting the edge emission of the LSC devices with a spectroradiometer (International Light Technologies ILT950) equipped with a cosine corrector. The emission spectra of the LSCs were recorded using Spectrilight software. A digital multimeter (KEITHLEY 2612B) was connected in series with the circuit, between the PV module and the potentiometer, to perform the voltage scans and measure the current output. PV tests were repeated both by placing an absorbing black background in contact with the LSC rear side to avoid photocurrent overestimation due to photon double-pass effects, and by fixing a white diffuser (Edmund Optics, #34-480) in contact with the back surface of the LSC to allow back scattering of transmitted photons. In both experimental setups, a black mask placed on the front face of the LSC system was used to avoid direct illumination of the PV cells. These photocurrent measurements allowed to determine the device efficiency of LSC-PV assembly. All the above cited tests were repeated for at least three devices.

Both **2**/PMMA and **3**/PMMA coating with optimized concentration was subjected to weathering tests under continuous Xenon light illumination and aerobic conditions. The total irradiance was measured with the spectroradiometer and set at approximately 1000 $W \cdot m^{-2}$ (600 $W \cdot m^{-2}$ in the 300-800 nm wavelength range and 12 $W \cdot m^{-2}$ in the 295-400 nm range) for the entire duration of the test. The relative humidity and the working temperature inside the testing chamber were maintained constant and measured to be 35% and 45 °C, respectively. The normalized trend for integrated single-edge optical power output was calculated by dividing the value measured at a given exposure time by the value measured at 0 h of exposure. Accelerated aging tests were also performed in combination with

UV–vis and fluorescence spectroscopy to assess the photostability of the PFPBNT in THF–H_2O mixture with f_w equal to 75% under UV-A irradiation (54.6 mW cm^{-1}) and at a temperature of 50 °C.

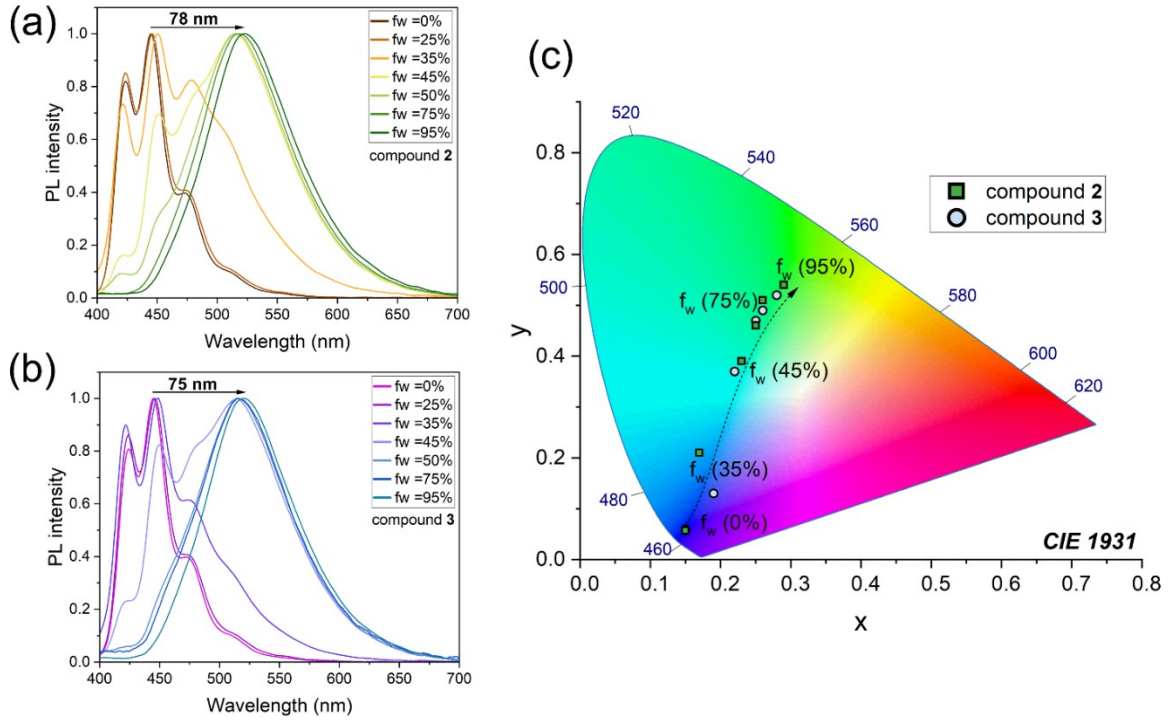

Figure S19. Stokes shift for emission from THF solutions for compounds **2** and **3** with increasing amounts of water and (c) CIE 1931 chromaticity diagram of **2** and **3** in THF/H_2O mixtures.

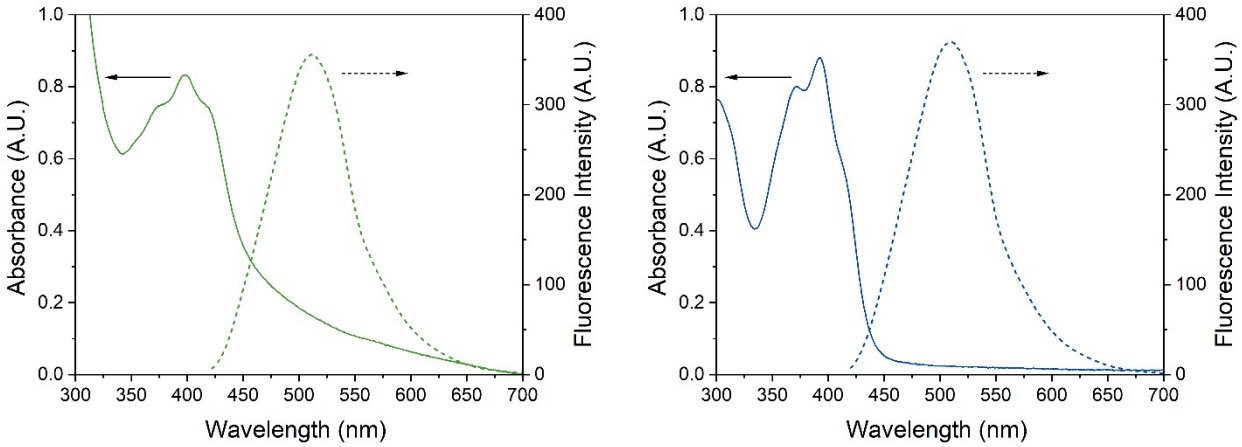

Figure S20. Absorption and emission upon excitation at 370 nm of **2**/PMMA (left, green line) and **3**/PMMA (right, blue line) coatings.

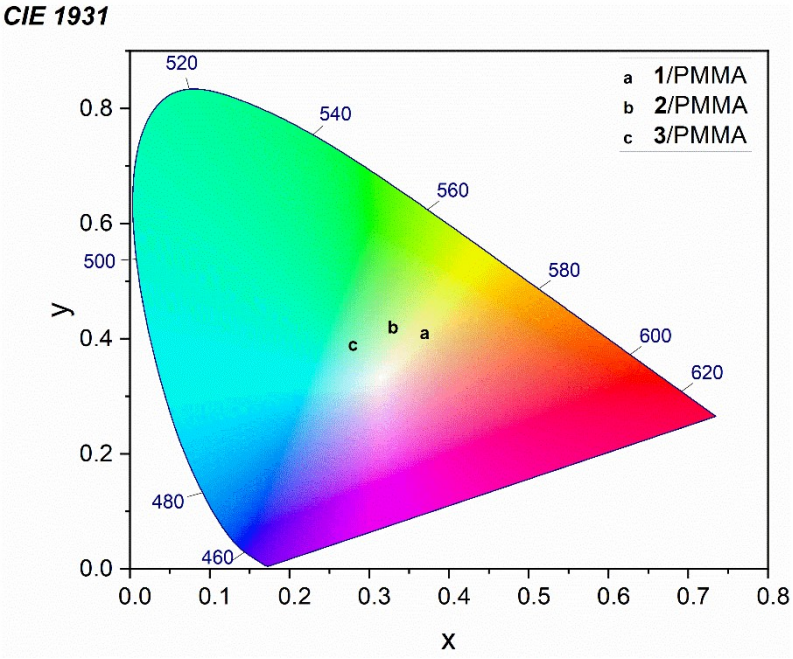

Figure S21. Color coordinates (CIE 1931 Uniform Color Space) of AIEgens/PMMA LSC systems.

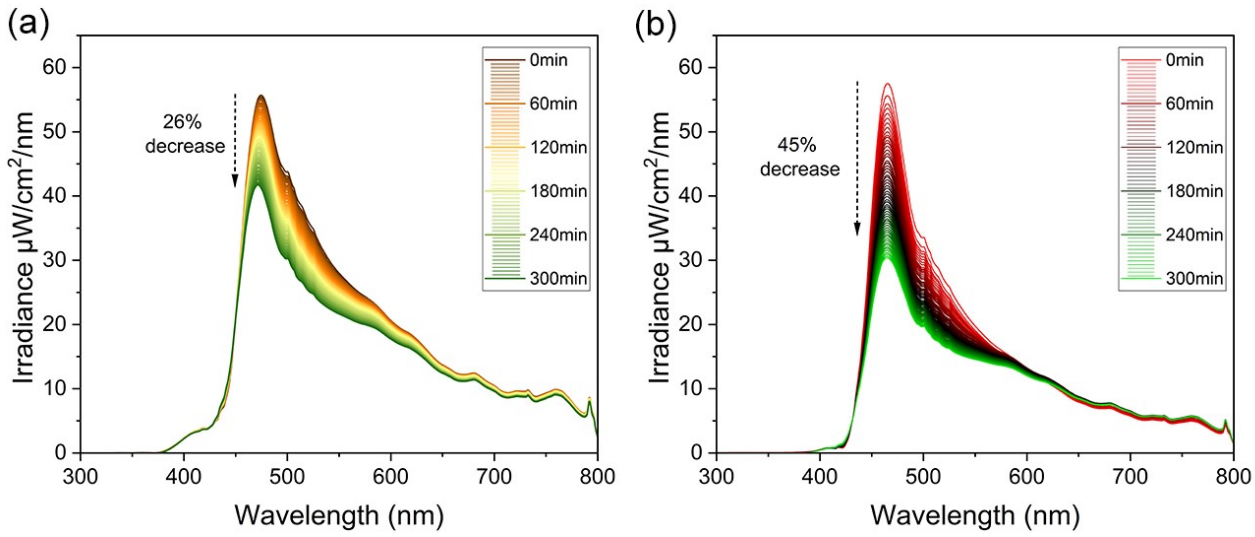

Figure S22. Single edge output of **2**/PMMA (a) and **3**/PMMA(b) monitored every 5 minutes for a total of 300 minutes (5hours) under continuous irradiation with solar simulated light (100 mW·cm^{-2}).

Photonic Analysis. To characterize the optical performance of LSCs as photonic systems, two parameters were used, namely the external photon efficiency (η_{ext}) and the internal photon efficiency (η_{int}) (**Equation S1** and **S2**):

$$\eta_{ext} = \frac{N_{ph-out}}{N_{ph-in}} = \frac{Nº\ of edge\ emitted\ photons}{Nº\ of\ incident\ photons} = \frac{\sum_{i=1300}^{4}\int^{800} P_{i(out)}(\lambda)\frac{\lambda}{hc}d\lambda}{\sum_{i=1300}^{4}\int^{800} P_{(in)}(\lambda)\frac{\lambda}{hc}d\lambda} \#(S1)$$

$$\eta_{int} = \frac{N_{ph-out}}{N_{ph-abs}} = \frac{Nº\ of\ edge\ emitted\ photons}{Nº\ of\ absorbed\ photons} = \frac{\sum_{i=1300}^{4}\int^{800} P_{i(out)}(\lambda)\frac{\lambda}{hc}d\lambda}{\sum_{i=1300}^{4}\int^{800} P_{(in)}(\lambda)\frac{\lambda}{hc}(1-10^{-A(\lambda)})d\lambda} \#(S2)$$

where $N_{ph\text{-}out}$ is the total number of edge-emitted photons summed over four edges (i = 1-4) of the LSC, $N_{ph\text{-}abs}$ is the total number of photons absorbed by the LSC, and $N_{ph\text{-}in}$ is the total number of photons incident on the top surface of the LSC. Also, h is Planck's constant (in J s) and c is the speed of light (in m s^{-1}). $N_{ph\text{-}out}$ is obtained from the sum of the output power spectra, $P_{i(out)}(\lambda)$, measured for each edge of the LSC (in W nm^{-1}), where λ is the wavelength of light (in nm). $P_{in}(\lambda)$ is the input power spectrum from the solar simulator incident on the top surface of the LSC (in W nm^{-1}).

The absorption efficiency (η_{abs}), instead, is defined as the fraction of absorbed incident photons of the available photon flux. It is given by **Equation S3**:

$$\eta_{abs} = \frac{\int_0^{\infty} S_{SO}(\lambda)\,[1-10^{-\mathrm{A}(\lambda)}]\,d\lambda}{\int_0^{\infty} S_{SO}(\lambda)d\lambda} \#(S3)$$

Photovoltaic characterization. To assess the performance of the assembled LSC-PV system with optimum AIEgen concentration (12.5 wt%), photocurrent measurements were accomplished after coupling two c-Si PV modules to two opposite edges of the LSC. The power conversion efficiency (η_{dev}) was determined as the electrical power effectively extracted from the PV cells (P_{el}^{out}) relative to the optical input power hitting the top surface of the LSC (P_{opt}^{in}), as reported in Equation S4 below:

$$\eta_{dev} = \frac{P_{el}^{out}}{P_{opt}^{in}} = \frac{FF\, I_{SC}\, V_{OC}}{P_{opt}^{in}\, A_{LSC}} \#(S4)$$

where FF, I_{SC} and V_{OC} are the fill factor, the short-circuit current and the open-circuit voltage of the edge-coupled PV cells, respectively, P in opt is the incident solar power density (in $mW \cdot cm^{-2}$) and A_{LSC} is the front illuminated area of the LSC device (in cm^2).

The tests were carried out in the presence of a black absorbing background, as more precisely described in the Experimental Section. The complete data collected (V_{OC}, I_{SC}, FF, P_{max}, and η_{dev}) are reported in Table S4.

Table S4. Voc, Isc, FF, P_{max} and η_{dev} calculated for **1-3**/PMMA LSC-PV assemblies at 12wt% concentration

	V_{OC} [V]	**I_{SC} [mA]**	**FF**	**P_{max} [mW]**	**η_{dev} [%]**
1/PMMA	1.83 ± 0.03	4.46 ± 0.05	0.56 ± 0.01	4.75 ± 0.02	0.186 ± 0.004
2/PMMA	1.81 ± 0.01	4.65 ± 0.04	0.55 +0.01	4.04 ± 0.05	0.185 ± 0.004
3/PMMA	1.84 ± 0.01	4.90 ± 0.03	0.52 ± 0.01	4.25 ± 0.08	0.188 ± 0.002

6. Spectra of new compounds

Compound **1**

^{1}H NMR (400 MHz, $CDCl_3$)

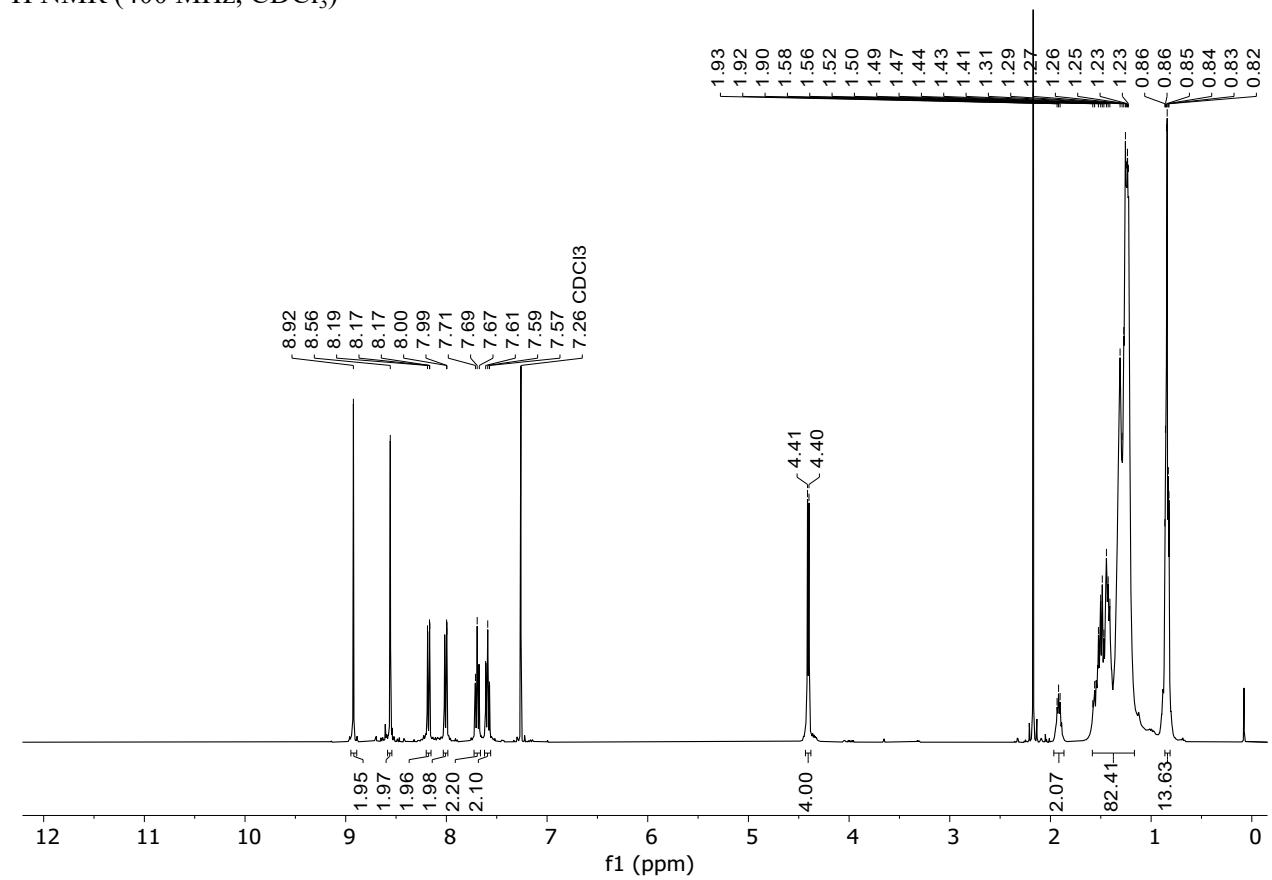

^{13}C NMR (101 MHz, $CDCl_3$)

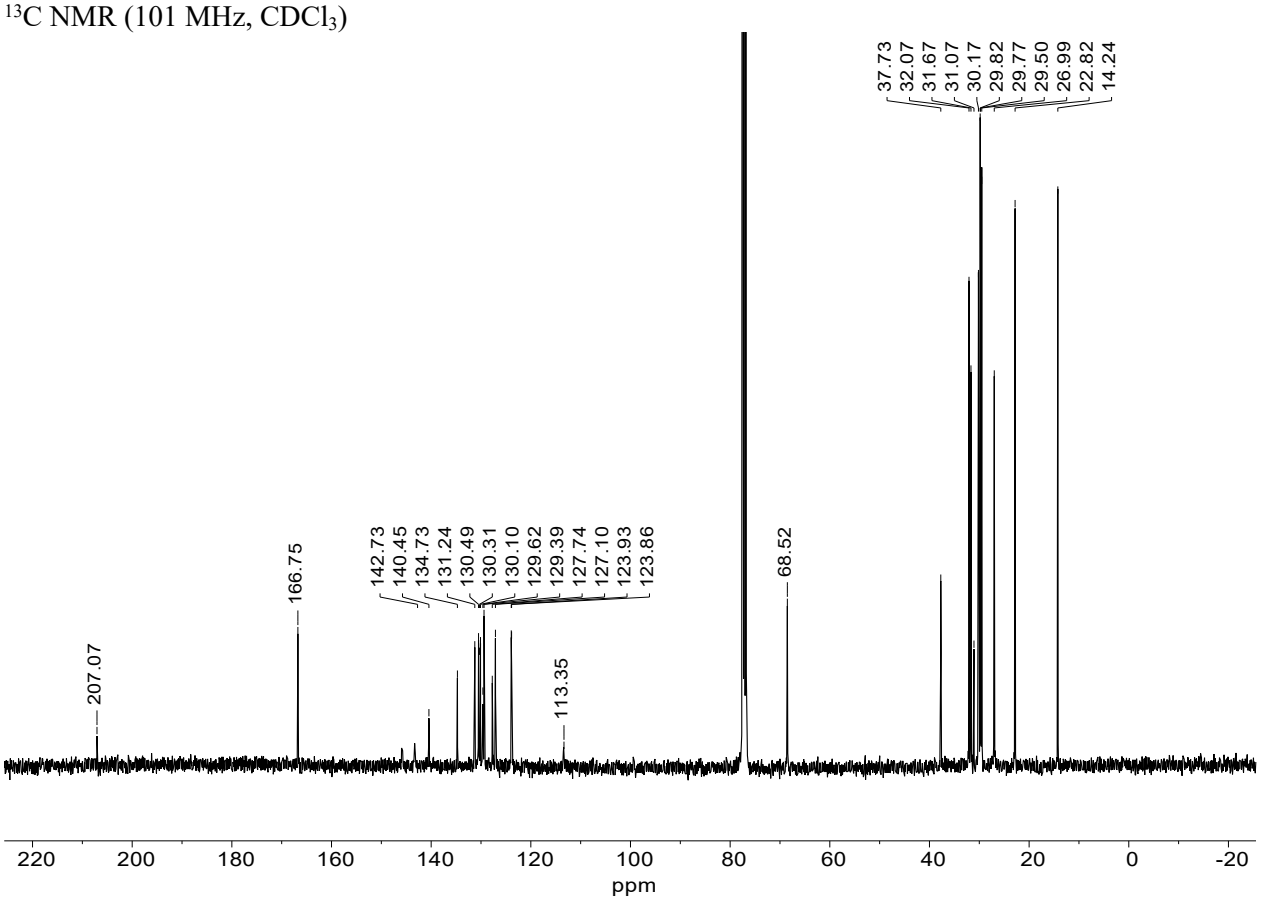

HRMS (ESI-ToF)

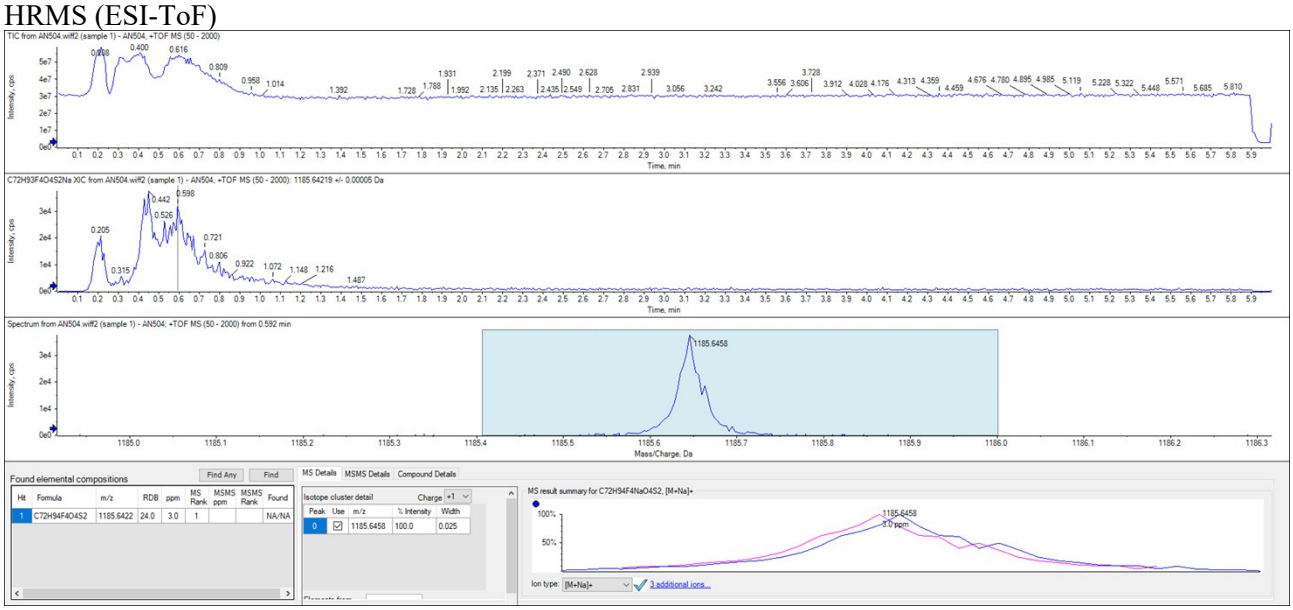
TIC from AN504.wiff2 (sample 1) - AN504, +TOF MS (50 - 2000)
Intensity, cps
Time, min
C72H93F4O4S2Na XIC from AN504.wiff2 (sample 1) - AN504, +TOF MS (50 - 2000): 1185.64219 +/- 0.00005 Da
Intensity, cps
Time, min
Spectrum from AN504.wiff2 (sample 1) - AN504, +TOF MS (50 - 2000) from 0.592 min
1185.6458
Intensity, cps
Mass/Charge, Da
Found elemental compositions
Find Any
Find
Hit
Formula
m/z
RDB
ppm
MS Rank
MSMS ppm
MSMS Rank
Found
1
C72H94F4O4S2
1185.6422
24.0
3.0
1
NA/NA
MS Details
MSMS Details
Compound Details
Isotope cluster detail
Charge
+1
Peak
Use
m/z
% Intensity
Width
0
1185.6458
100.0
0.025
MS result summary for C72H94F4NaO4S2, [M+Na]+
1185.6458
3.0 ppm
100%
50%
Ion type:
[M+Na]+
3 additional ions...

Compound **2**

^{1}H NMR (400 MHz, $CDCl_3$)

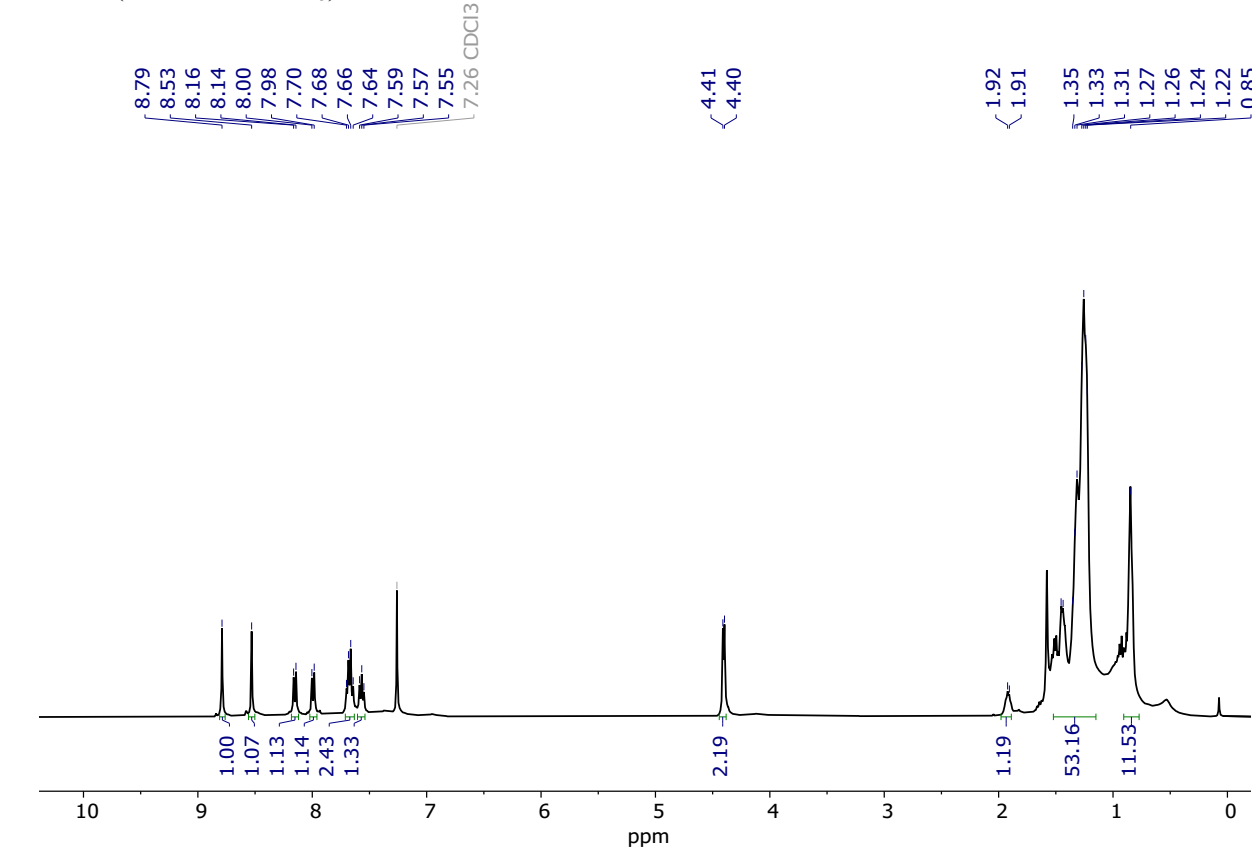

^{13}C NMR (101 MHz, $CDCl_3$)

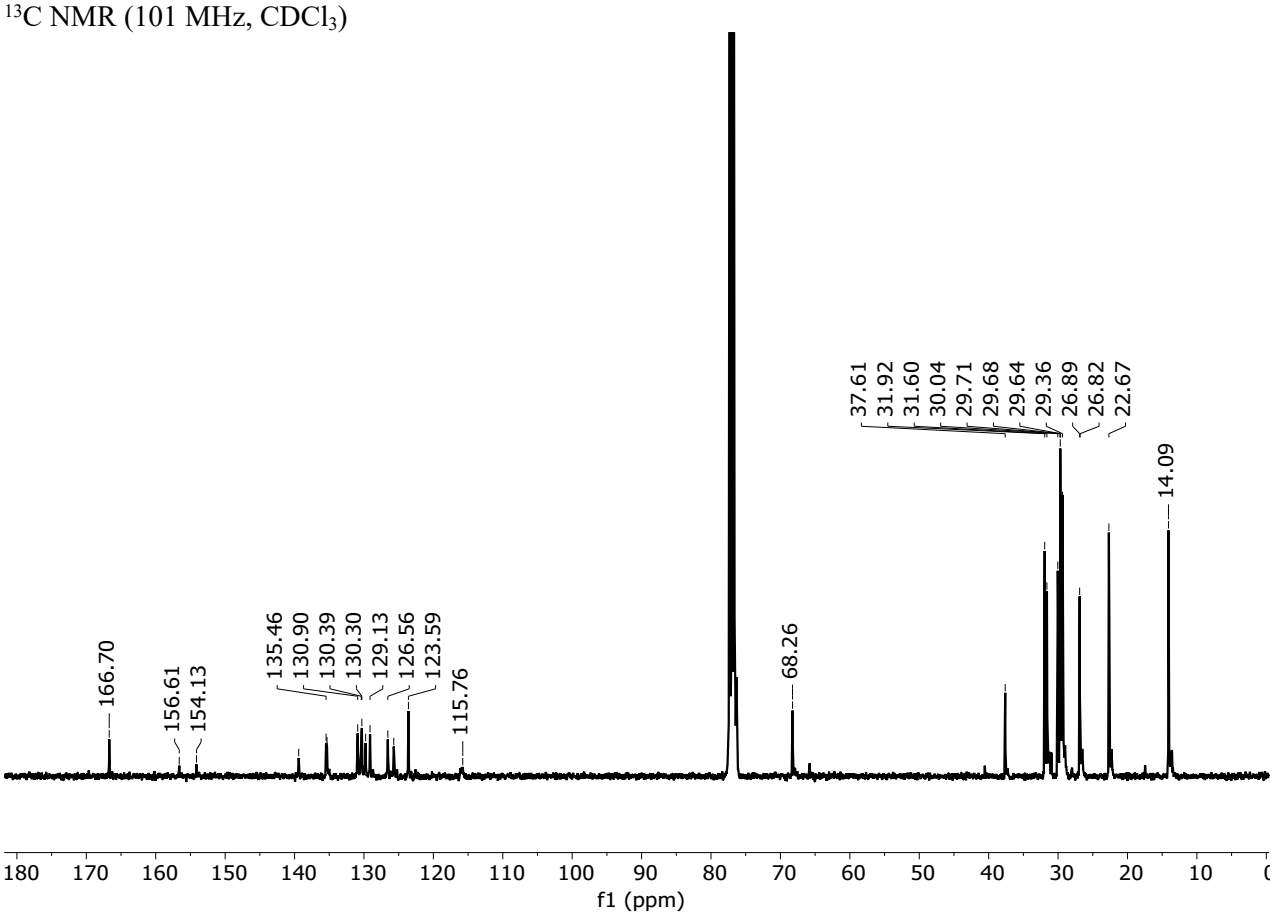

COSY

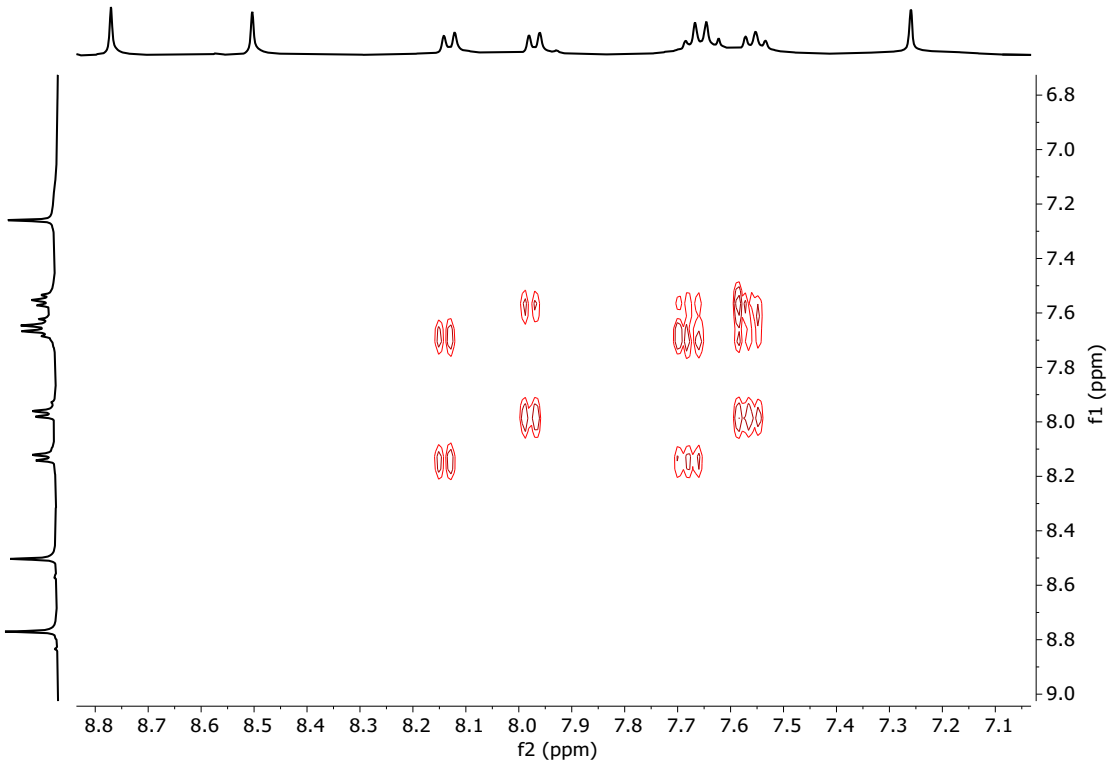
6.8
7.0
7.2
7.4
7.6
7.8
8.0
8.2
8.4
8.6
8.8
9.0
f1 (ppm)
8.8 8.7 8.6 8.5 8.4 8.3 8.2 8.1 8.0 7.9 7.8 7.7 7.6 7.5 7.4 7.3 7.2 7.1
f2 (ppm)

HSQC

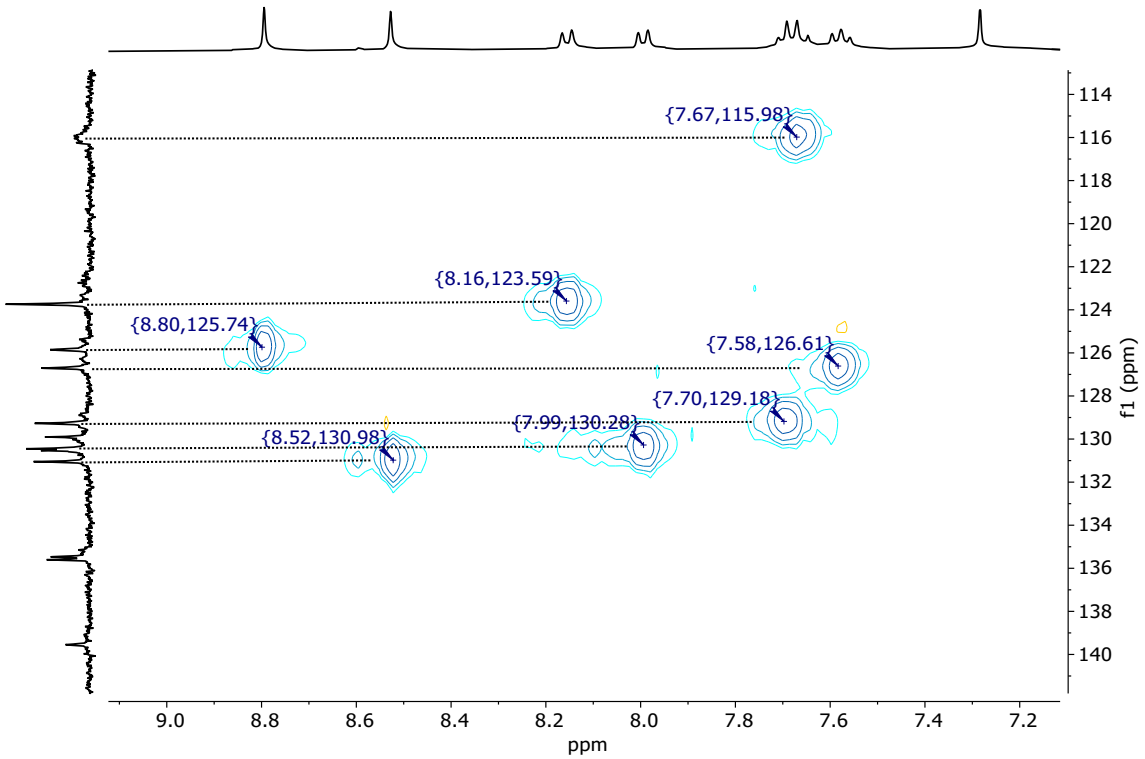
{7.67,115.98}
{8.16,123.59}
{8.80,125.74}
{7.58,126.61}
{7.70,129.18}
{7.99,130.28}
{8.52,130.98}
114
116
118
120
122
124
126
128
130
132
134
136
138
140
f1 (ppm)
9.0 8.8 8.6 8.4 8.2 8.0 7.8 7.6 7.4 7.2
ppm

HRMS (ESI-ToF)

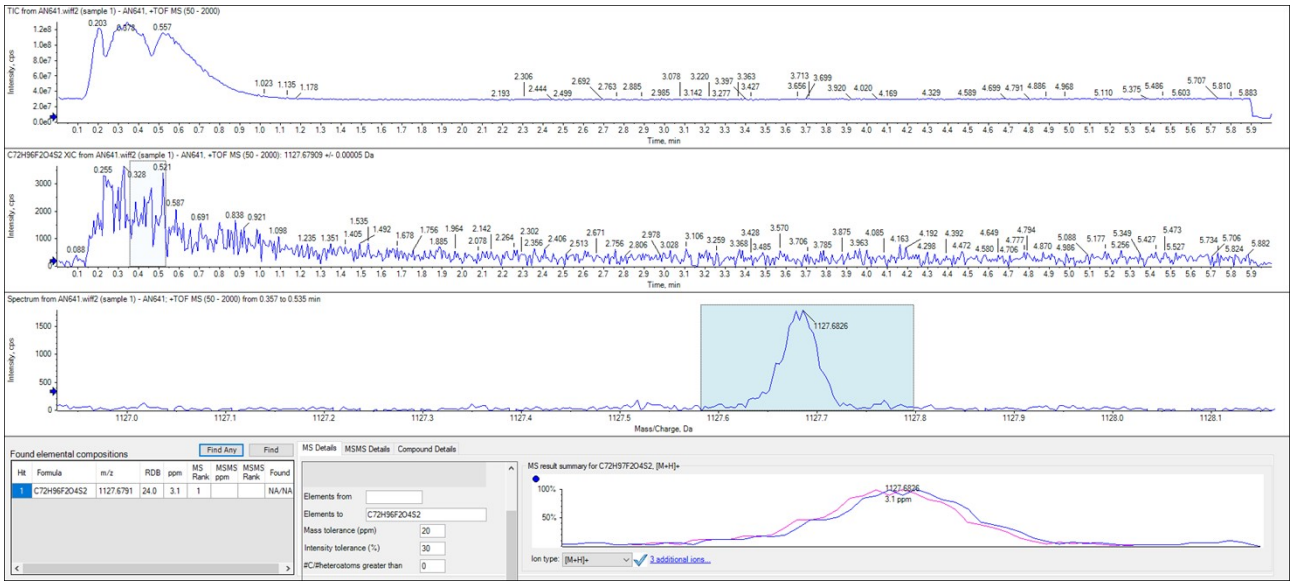
TIC from AN641.wiff2 (sample 1) - AN641, +TOF MS (50 - 2000)
Intensity, cps
Time, min
C72H96F2O4S2 XIC from AN641.wiff2 (sample 1) - AN641, +TOF MS (50 - 2000): 1127.67909 +/- 0.00005 Da
Intensity, cps
Time, min
Spectrum from AN641.wiff2 (sample 1) - AN641, +TOF MS (50 - 2000) from 0.357 to 0.535 min
1127.6826
Intensity, cps
Mass/Charge, Da
Found elemental compositions
Find Any
Find
Hit
Formula
m/z
RDB
ppm
MS Rank
MSMS ppm
MSMS Rank
Found
1
C72H96F2O4S2
1127.6791
24.0
3.1
1
NA/NA
MS Details
MSMS Details
Compound Details
Elements from
Elements to
C72H96F2O4S2
Mass tolerance (ppm)
20
Intensity tolerance (%)
30
#C/#heteroatoms greater than
0
MS result summary for C72H97F2O4S2, [M+H]+
100%
50%
1127.6826
3.1 ppm
Ion type:
[M+H]+
3 additional ions...

Compound **3**

^{1}H NMR (400 MHz, $CDCl_3$)

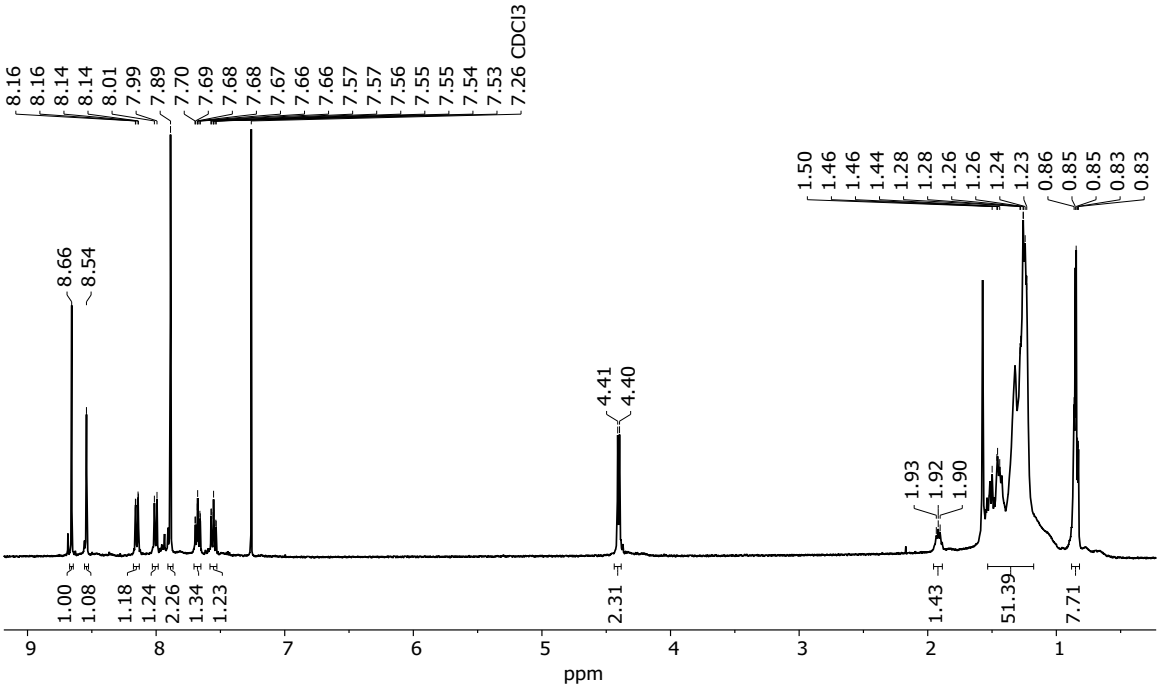

^{13}C NMR (101 MHz, $CDCl_3$)

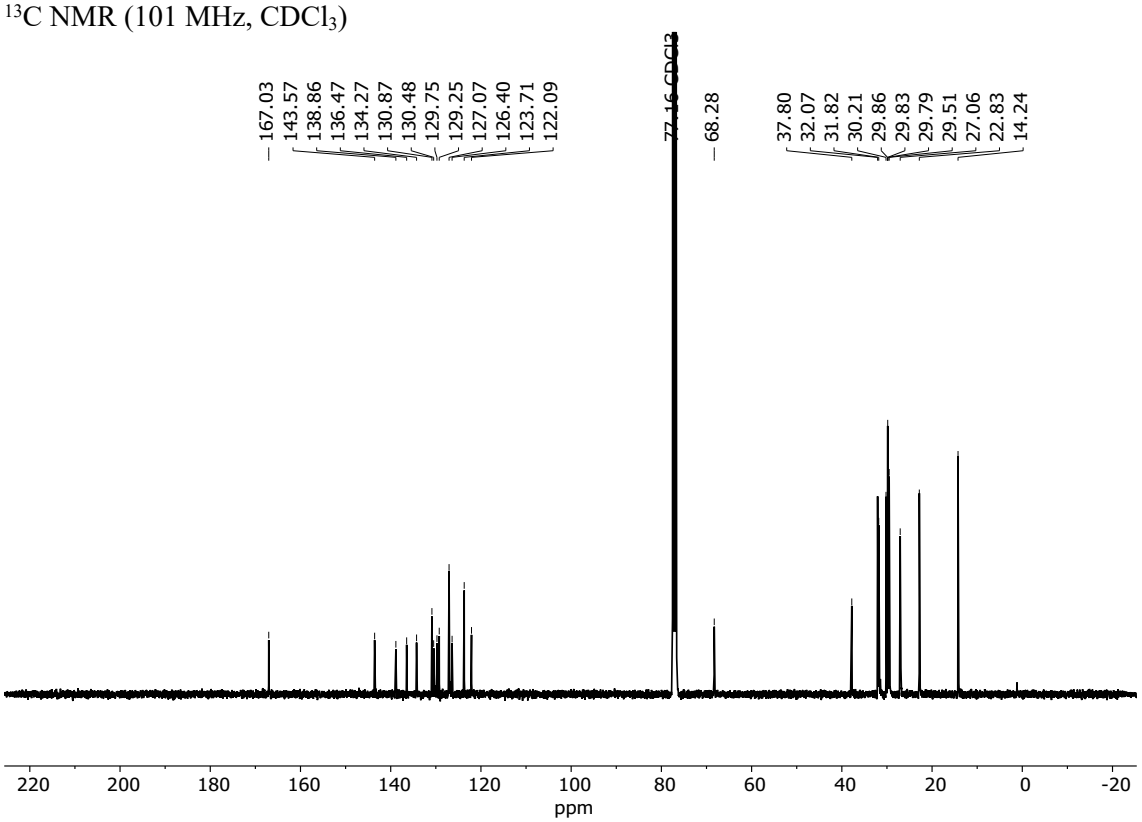

COSY

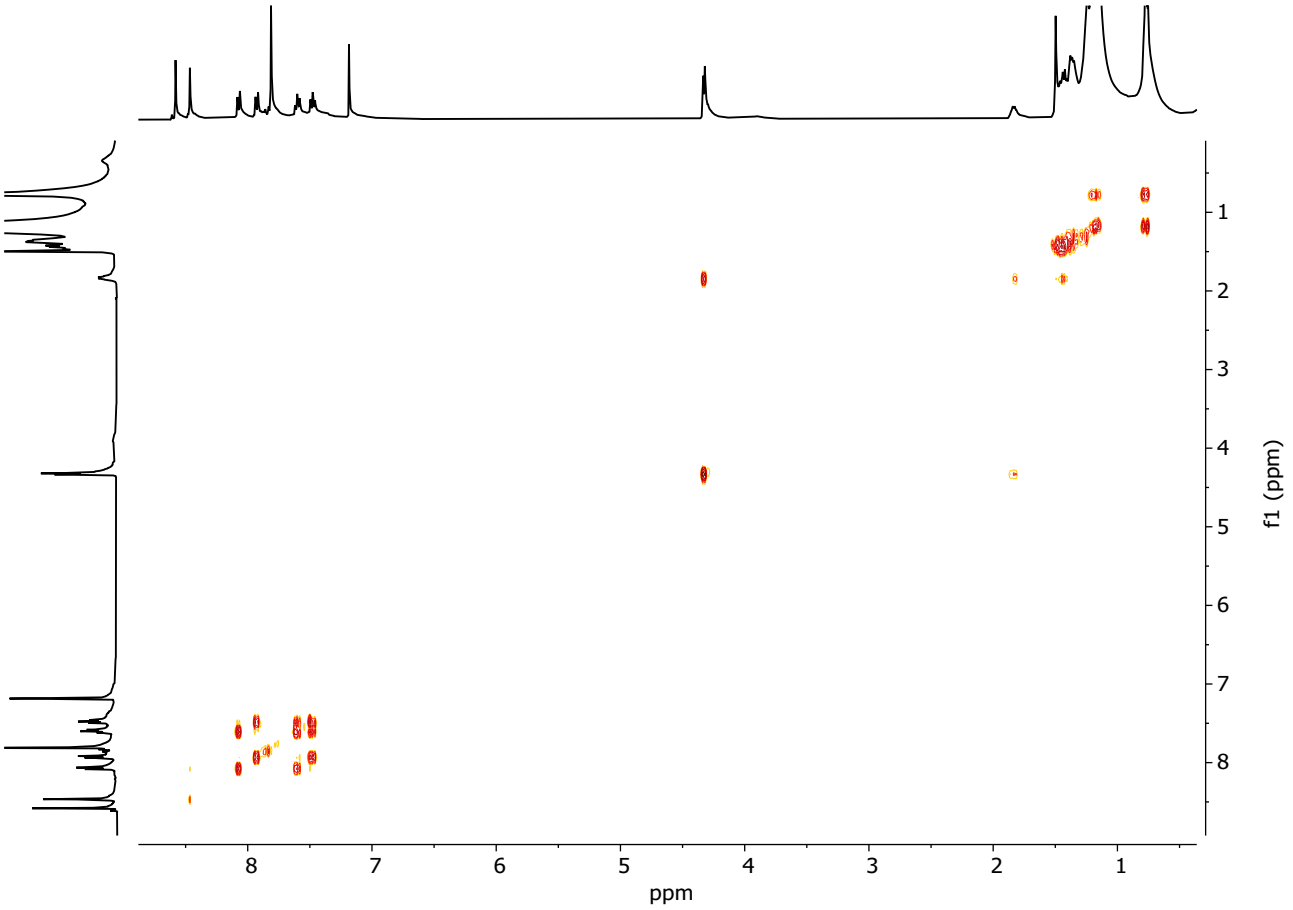

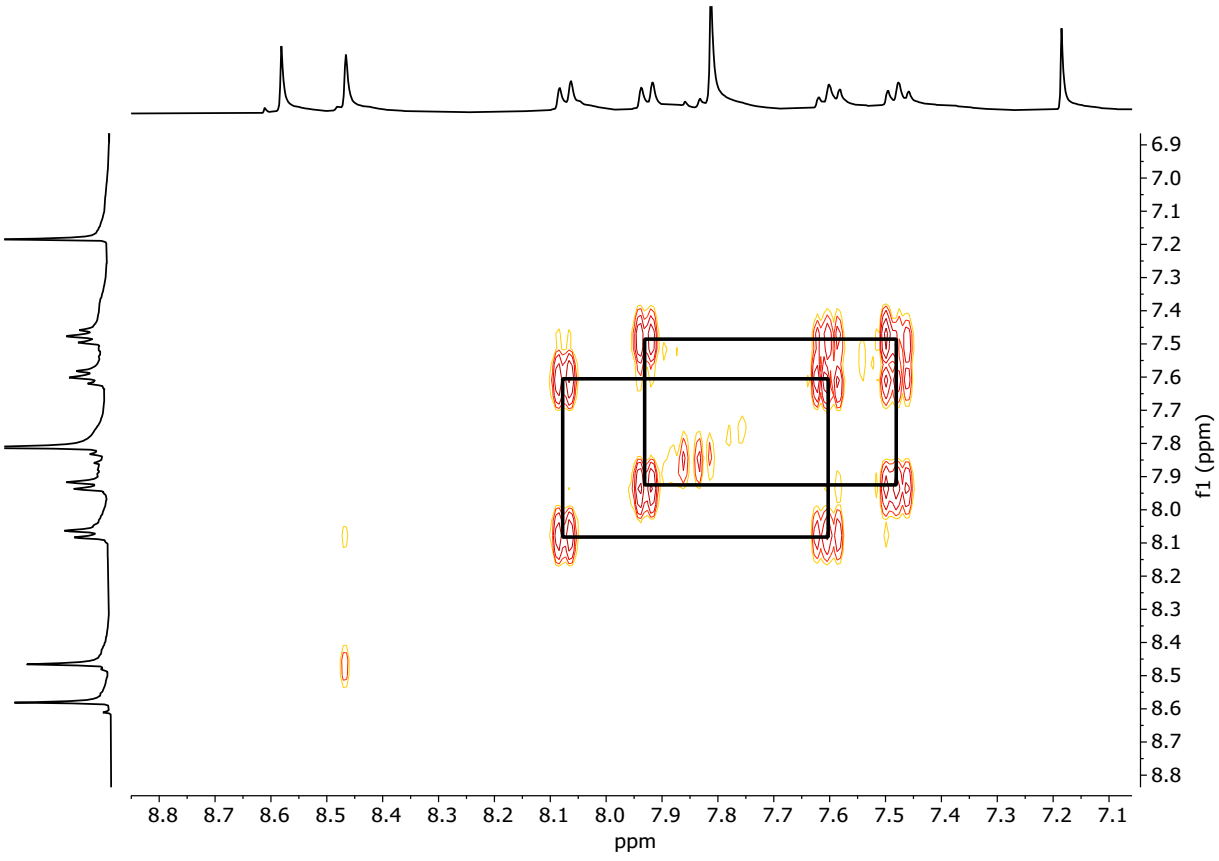

HSQC

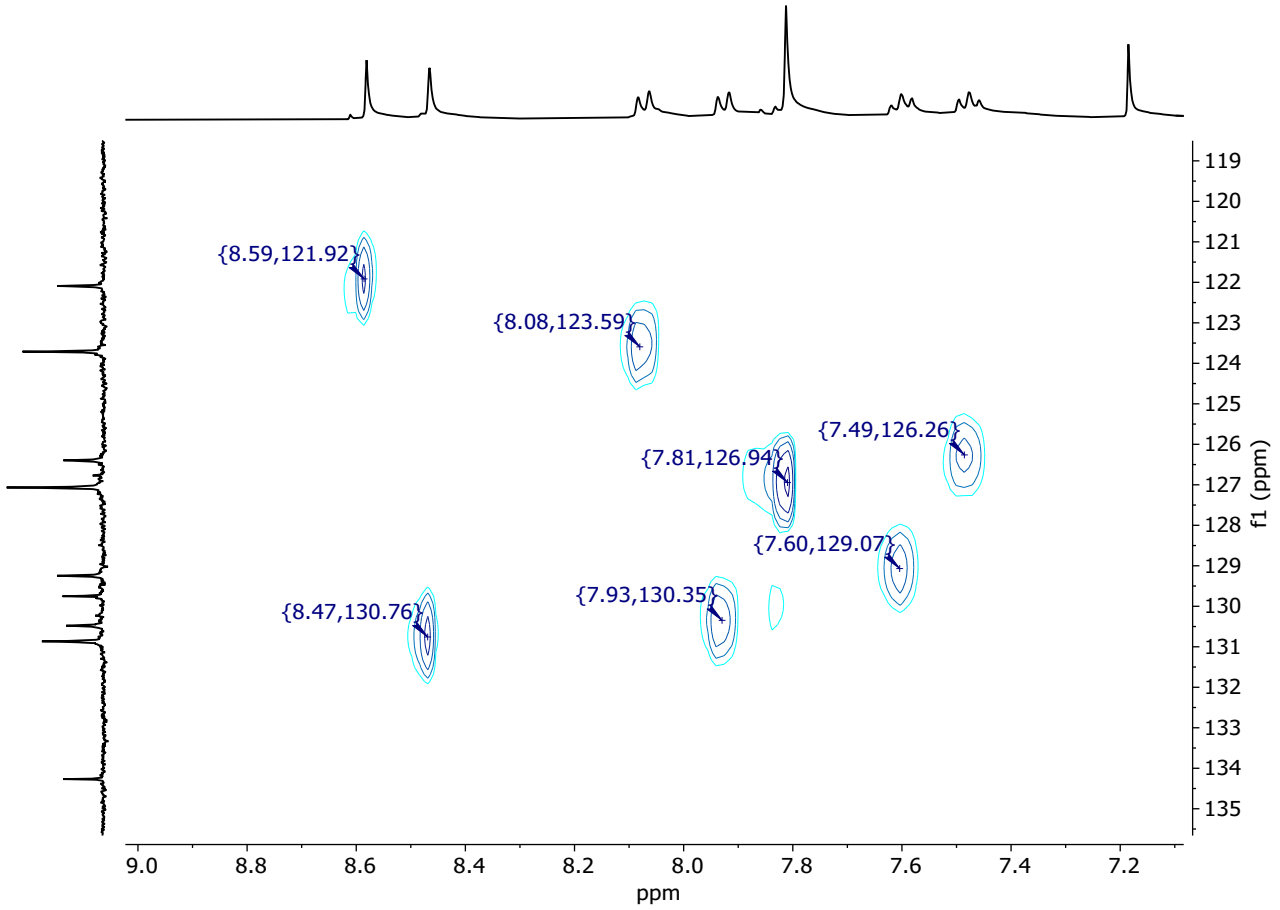

HRMS (ESI-ToF)

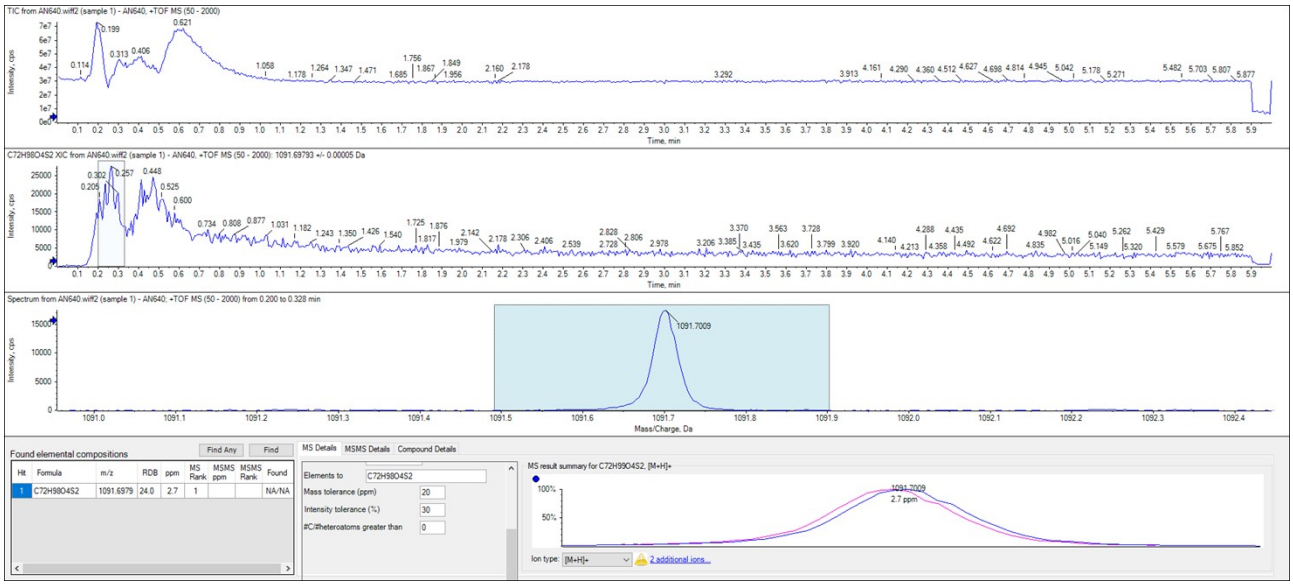

7. References

[S1] A. Nitti, G. Bianchi, R. Po and D. Pasini, *Synthesis*, 2019, **51**, 677–682.

[S2] A. Nitti, G. Forti, G. Bianchi, C. Botta, F. Tinti, M. Gazzano, N. Camaioni, R. Po and D. Pasini, *J. Mater. Chem. C*, 2021, **9**, 9302–9308.

[S3] F. Corsini, A. Nitti, E. Tatsi, G. Mattioli, C. Botta, D. Pasini and G. Griffini, *Adv. Opt. Mater.*, 2021, **9**, 2100182.

[S4] P. Pracht, F. Bohle, S. Grimme, *Phys. Chem. Chem. Phys.*, 2020, **22**, 7169.

[S5] C. Bannwarth, S. Ehlert and S. Grimme, *J. Chem. Theory Comput.*, 2019, **15**, 1652–1671; S. Grimme, *J. Chem. Theory Comput.*, 2019, **15**, 2847–2862.

[S6] F. Neese, *WIREs Comput Mol Sci*, 2012, **2**, 73–78; F. Neese, *WIREs Comput Mol Sci*, 2022, 12, e1606.

[S7] F. Weigend and R. Ahlrichs, *Phys. Chem. Chem. Phys.*, 2005, **7**, 3297; A. Schäfer, H. Horn and R. Ahlrichs, *J. Chem. Phys.*, 1992, **97**, 2571–2577.

[S8] V. Barone and M. Cossi, *J. Phys. Chem. A*, 1998, **102**, 1995–2001.

[S9] S. Ehlert, U. Huniar, J. Ning, J. W. Furness, J. Sun, A. D. Kaplan, J. P. Perdew and J. G. Brandenburg, *J. Chem. Phys.*, 2021, **154**, 061101.

[S10] A. D. Becke, *J. Chem. Phys.*, 1992, **96**, 2155–2160.

[S11] E. Caldeweyher, S. Ehlert, A. Hansen, H. Neugebauer, S. Spicher, C. Bannwarth and S. Grimme, *J. Chem. Phys.*, 2019, **150**, 154122.

[S12] B. De Souza, F. Neese and R. Izsák, *J. Chem. Phys.*, 2018, **148**, 034104.